1993ApJ...419..524M

THE ASTROPHYSICAL JOURNAL, 419:524–540, 1993 December 20
© 1993. The American Astronomical Society. All rights reserved. Printed in U.S.A.

THE ENVIRONMENT OF LYMAN-α ABSORBERS IN THE SIGHT LINE TOWARD 3C 273

S. L. MORRIS,[1] R. J. WEYMANN, ALAN DRESSLER, AND P. J. MCCARTHY
The Observatories of the Carnegie Institution of Washington, 813 Santa Barbara Street, Pasadena, CA 91101
B. A. SMITH
Institute for Astronomy, University of Hawaii, Honolulu, HI 96822
R. J. TERRILE
Jet Propulsion Laboratory, Pasadena, CA 91109
R. GIOVANELLI
Department of Astronomy and National Astronomy and Ionosphere Center,[2] Cornell University, Ithaca, NY 14853
AND
M. IRWIN
Royal Greenwich Observatory, Madingley Road, Cambridge CB3 0EZ, UK
Received 1993 March 15; accepted 1993 June 29

ABSTRACT

We present new ground-based data following up on the *Hubble Space Telescope* discovery of low-redshift Lyα absorption in the sight line to the quasar 3C 273. Our goal is to investigate the relationship between the low column density absorbers and higher column density objects such as galaxies or H II regions. Narrow-band filter observations with a coronagraph show that there are no H II regions or other strong Hα line–emitting gas within a 12 kpc radius of the line of sight to the quasar, at the velocities of three of the absorbers. Broad-band imaging in Gunn *r* shows that there are no dwarf galaxies at Virgo distances with absolute magnitude above $M_B \approx -13.5$ and within a radius of 40 kpc from the line of sight to the quasar. Finally, we present fiber spectroscopy of a complete sample of galaxies within a radius of 1°, down to an apparent magnitude of $B \approx 19$. Analysis of this sample, combined with galaxies within 10 Mpc of the quasar line of sight taken from the literature, shows that the absorbers are definitely not distributed at random with respect to the galaxies, but also that the absorber-galaxy correlation function is not as strong as the galaxy-galaxy correlation function on large scales. We show that our data are consistent with the hypothesis that all galaxies more luminous than $0.1L^*$ have effective cross sections [for association with absorbers whose neutral hydrogen column density ($\log N_{\rm H\,I}$) is greater than 13.0] of between 0.5 and 1 Mpc. We also show a clear case of a Lyα absorber which has no galaxy brighter than $M_B = -18$ within a projected distance of 4.8 Mpc, and discuss the possibility that Lyα absorbers are destroyed in a rich galaxy environment.

Subject headings: intergalactic medium — quasars: absorption line — quasars: individual (3C 273)

1. INTRODUCTION

Understanding the origin and evolution of structure in the universe remains one of the most fundamental and active challenges of current astrophysical research. As the evidence in favor of a cosmological origin for the narrow, displaced absorption lines in QSO spectra became overwhelming, it also became clear that both the metal-line systems and the Lyα systems are invaluable tools for the study of some aspects of the problem. Since ground-based Lyα studies refer only to redshifts $\gtrsim 1.6$, they complement studies of galaxy clustering properties, the majority of which involve redshifts much less than this. However, precisely because the redshift regimes have been so different and because it has not been at all clear what relation exists between the typical low column density Lyα absorbers and galaxies, these two approaches have remained disjoint. It was somewhat unexpected, but pleasing, that low-redshift Lyα absorbers were found in sufficient numbers to enable meaningful studies of the evolution of the Lyα absorbers and their relation to galaxies (Morris et al. 1991; Bahcall et al. 1991b). This has presented astronomers with the opportunity to join these two lines of investigation.

There are two levels at which such attempts can be carried out: (1) purely statistical investigations aimed at comparing the clustering properties of galaxies and Lyα absorbers, and (2) investigation of individual cases in which the possibility of establishing the presence (or absence) or a clear link between the Lyα absorption line and something we could call a "galaxy" presents itself. Preliminary discussions along these lines may be found in papers by Bahcall et al. (1992a, b) and by Salzer (1992). The present paper is a first attempt to pursue both these approaches along the sight line to 3C 273. The remainder of this paper is organized as follows: In § 2 we describe the different sets of observations we have assembled to investigate the environment of the Lyα absorbers along the 3C 273 sight line. In § 3 we analyze them for possible associations or lack of associations of individual Lyα absorbers with galaxies, and also give some statistical analysis of the clustering properties of the Lyα absorbers with galaxies. In § 4 we discuss these results in light of current models of the Lyα absorbers and provide a brief summary and suggestions for further work.

Throughout this paper H_0 is taken to be 80 km s^{-1} Mpc^{-1}, the distance of the Virgo Cluster is taken to be 16.0 Mpc [a

[1] Present address: Dominion Astrophysical Observatory, 5071 West Saanich Road, Victoria, BC, Canada V8X 4M6.

[2] The National Astronomy and Ionosphere Center is operated by Cornell University under a cooperative agreement with the US National Science Foundation.

© American Astronomical Society • Provided by the NASA Astrophysics Data System

1993ApJ...419..524M

distance modulus of $(m - M)_{\rm Virgo} = 31.02$; Jacoby et al. 1992], and q_0 is taken to be zero.

2. OBSERVATIONS AND REDUCTION

It has long been realized that imaging of the gas directly responsible for the low column density Lyα absorbers is well beyond the reach of current technology. Specifically, the neutral hydrogen column densities of order 10^{13}–10^{14} cm^{-2} detected by the Goddard High Resolution Spectrograph (GHRS) toward 3C 273 are about four or five orders of magnitude below what can be imaged in 21 cm emission, even without taking into account the powerful radio background contributed by 3C 273 itself. The Hα recombination surface brightness associated with these neutral hydrogen column densities is also several orders of magnitude below what is feasible to detect, unless the incident flux of ionizing photons is several orders of magnitude higher than that expected from the integrated background radiation.

However, it has frequently been suggested that the Lyα absorbers are intimately connected with, or are actual extensions of, entities which *can* be imaged by means of either Hα emission, starlight, or 21 cm emission—e.g., dwarf galaxies (Fransson & Epstein 1982) or shells of expanding gas (Chernomordic & Ozernoy 1983) or the outer regions of galactic disks (Maloney 1992). In the case of dwarf irregulars, for example, a very small episode of recent star formation might betray the presence of a dwarf irregular whose outer envelope produces the Lyα absorbers. Alternatively, expanding shells of gas might produce Hα emission via collisional ionization at a shock front.

In addition, of course, possible association of individual Lyα absorbers with specific galaxies, as well as statistical studies of absorber-galaxy correlation, can be carried out with a sample of redshifts for galaxies in the field surrounding 3C 273.

In this section we describe three such new sets of observations of a region centered on 3C 273. These are (§ 2.1) coronagraph observations with narrow-band filters of a 5′ diameter region, (§ 2.2) deep broad-band imaging of a 17′ diameter region, and (§ 2.3) fiber spectroscopy of a 2°.2 × 1°.6 region down to a limiting magnitude of $B = 19$. We describe the analysis of these sets of observations in § 3.

2.1. *Coronagraph Observations with Narrow-Band Filters*

Observations of a 5′.3 × 5′.3 region (radius ≈ 12 kpc at Virgo) around 3C 273 were obtained during 1992 February 3–7, with the University of Hawaii Coronagraph (Vilas & Smith 1987) on the Las Campanas 2.5 m du Pont Telescope. A thinned 1024 × 1024 Tektronics CCD was used, binned 2 × 2, giving a scale of 1″.23 pixel^{-1}. The coronagraph blocking mask had a diameter of 5″. Data were obtained with a Gunn *r* filter, and also five specially acquired filters, three with width 13.5 Å, centered at 6586.2, 6598.0, and 6756.0 Å (hereafter referred to as VN1, VN2, and HN), and two with width 25 Å, centered at 6643.2 and 6718.9 Å (hereafter referred to as VB and HB). (The above widths and central wavelengths are quoted for an f/7.5 beam and a temperature of 15° C.) The narrow-band wavelengths were chosen to match the redshifted position of Hα at the velocities of the two Lyα absorbers listed in Morris et al. (1991) at velocities corresponding to the Virgo Cluster (Binggeli, Sandage, & Tammann 1985), and one absorber at 1251 Å. This is the lowest redshift strong Lyα system beyond the Virgo Cluster. The observing procedure involved cycling through the six different filters with exposure times of 10 minutes for the *r* and 25 Å filters and 20 minutes for the 13.5 Å filters. Seven such cycles were completed over the five-night run. During the observing run, it was discovered that the narrow-band filter HN had slightly nonparallel faces, resulting in detectable "ghost" images offset from bright stars and also 3C 273. In an attempt to minimize the effect of these, this filter was rotated through 90° between each night.

For calibration purposes, observations were also obtained of Mrk 49 (an emission-line galaxy in the Virgo Cluster with radial velocity 1524 km s^{-1}, and hence with Hα line emission within 2 Å of the peak of VN2) and M87, and also of a number of bright standard stars.

The images were reduced using the Interactive Reduction and Analysis Facility (IRAF).[3] The reduction steps were bias subtraction, division by a flat field taken on the same night as the observations, rotation and shifting of the images to match a reference image, sky subtraction, and averaging together of images taken with the same filter. It was found after the run that refocusing the coronagraph between taking the flat fields and the data meant that the flat-field division left significant features in the data, both at the edges of the coronagraph field and also throughout the data at the location of what are presumed to be dust particles on the coronagraph optics or CCD window. This problem was particularly noticeable for the data taken on the last night of the run. However, the residuals are greatly reduced in the combined data.

Continuum sources were removed from the narrow-band images by subtracting off a scaled version of the two 25 Å filter observations. We investigated scaling methods, including measuring stars or galaxies in the images, but found that the scaling derived was consistent with simply subtracting off the average of the 25 Å filters for each 13.5 Å observation. That is, there was no evidence for a significant continuum slope or calibration difference across the 150 Å region of interest, and the factor of 2 shorter broad-band exposure fairly accurately balanced the higher throughput of the 25 Å filters. This apparent consistency may be fortuitous, due to the small field (small number of galaxies) and the errors in measuring the flux of faint galaxies. Figure 1 shows the sum of the 25 Å data and the continuum-subtracted 13.5 Å data for 3C 273. As can be seen, the point spread function (PSF) is a function of angle off-axis, and becomes quite broad and asymmetric at the edge of the field, owing to aberrations in the coronagraph optics.

2.2. *Wide-Field Imaging with COSMIC*

A mosaic of Gunn *r*-band images of the field around 3C 273 was obtained on 1992 February 23, at the Palomar 5 m telescope, with the prime-focus COSMIC system. This recently commissioned camera contains a thinned 2048 × 2048 Tektronics CCD. Because of poor seeing, this was read out with 2 × 2 binning giving a scale of 0″.56 pixel^{-1}. Exposures were taken roughly centered on four positions offset from 3C 273 by 5′.4 northeast, northwest, southeast, and southwest. Four exposures of 5 minutes each were obtained at each position. During the observations, the Moon rose, and so the background level of the images varies by almost a factor of 2.

The data were reduced using IRAF. After bias subtraction, the data were flat-fielded using images of the dome. This left significant large-scale structure in the images, and so a

[3] IRAF is distributed by the National Optical Astronomy Observatories, which are operated by Associated Universities for Research in Astronomy, AURA, Inc., under contract to the National Science Foundation.

© American Astronomical Society • Provided by the NASA Astrophysics Data System

1993ApJ...419..524M

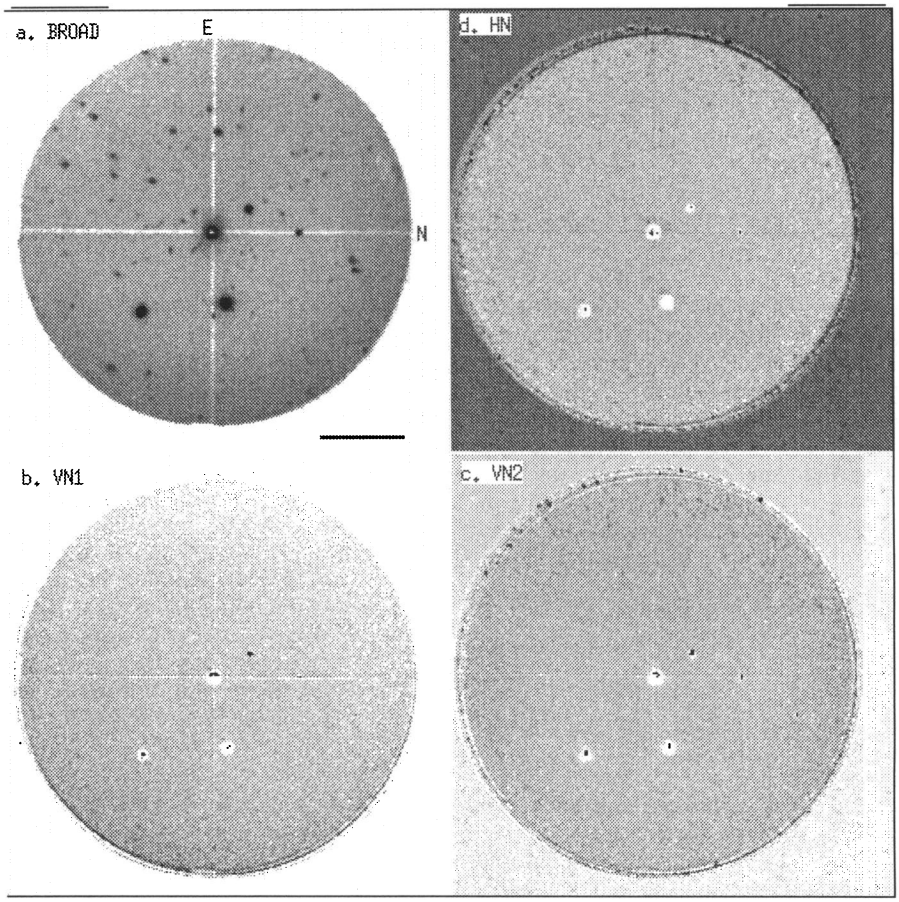

FIG. 1.—Coronagraph data for 3C 273 field. (*a*) Sum of 25 Å filters; the horizontal bar at lower right is 1′ long. (*b*) Continuum-subtracted VN1. (*c*) Continuum-subtracted VN2. (*d*) Continuum-subtraction HN. See text, § 2.1.

"skyflat" was constructed from the combined data images. This flat was median-smoothed to remove any small-scale structure. Because of a region of very low sensitivity near the center of the CCD, and also the location of a very bright star coincidentally at the same place in one set of images, the flat-fielded data still show a weak negative feature near the center of each image. The sky background was determined for each image separately and subtracted. The offsets between the images were determined by measuring the positions of the QSO and two bright nearby stars, which were common to all images, and the data were then mosaicked together, giving a combined image with diameter 17.2 centered on 3C 273. The resulting image is shown as Figure 2.

2.3. *Fiber Spectroscopy*

During 1992 February 8–10, spectra of objects in a 2.2 × 1.6 rectangle surrounding 3C 273 were obtained with the Fiber Spectrograph at the Las Campanas 2.5 m du Pont Telescope (Shectman 1992). This system has 128 fibers which are manually plugged into an aluminum plate over a 1.5 × 1.5 field. The fibers have a projected diameter of 3.″5. They feed the slit of a floor-mounted spectrograph. A 600 line mm^{-1} grating was used, with the 2D-FRUTTI photon-counting detector, giving a resolution of 8.6 Å FWHM. Three fields were observed for about 600 s each, offset east-west from each other.

Objects observed were chosen from a database produced by scanning a UKST IIIa-J plate of the region with the Automatic Plate Measuring Facility (APM) scanning machine at Cambridge. The APM produces a catalog of all the objects on a plate, with estimates of isophotal magnitudes, size, and a "sigma" parameter that measures how much the image parameters differ from those of stars with comparable magnitude. We chose objects to observe from this catalog with "sigma" > 3.0. This includes many fairly compact objects, and resulted in a rather high contamination by stars, but it also means that we found a number of compact galaxies that would otherwise have been missed. For each 1.5 × 1.5 fiber field, a magnitude-sorted list of candidate galaxies was produced. Because of restrictions on the minimum fiber separation, 330 out of a possible 336 object fibers were used, with 16 fibers per field set on blank sky.

The fiber spectra were extracted and reduced using the IRAF APEXTRACT package. The spectra were first traced and extracted. Then fiber-to-fiber throughput differences were corrected with a flat-field image, and the fibers were wavelength-calibrated and rebinned to a common linear wavelength scale. The wavelength calibration used an arc spectrum to determine the nonlinear relationship between wavelength and pixel number, after which a zero-point shift was measured for each fiber using the strong sky lines in the data. Finally, the sky emission was subtracted from each fiber using an unscaled template constructed from the 16 sky fibers in each frame.

Classification and radial velocity measurements for each spectrum were done in two ways. First each spectrum was

© American Astronomical Society • Provided by the NASA Astrophysics Data System

1993ApJ...419..524M

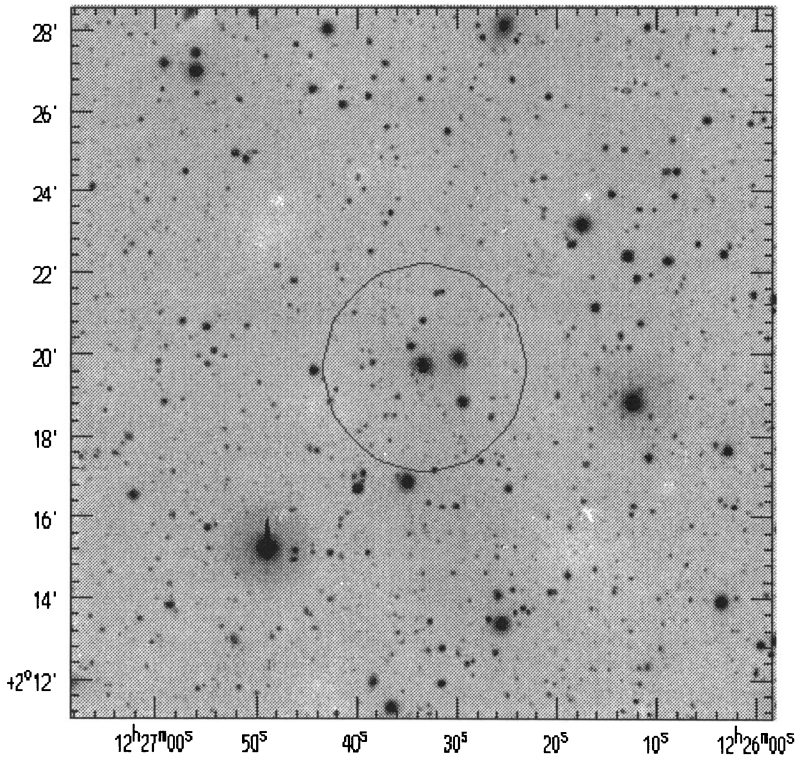

FIG. 2.—Mosaic of COSMIC images in Gunn *r* of 3C 273 field. See text, § 2.2. Region shown in Fig. 1 is circled.

inspected by eye and classified as either a star, a galaxy, or unknown. Then a radial velocity was determined by measuring either the position of the 4000 Å break or that of the [O II] λ3727.6 feature (actually a doublet, but unresolved in our data). A subjective assessment was also made of the reliability of the resulting radial velocity, dividing the sample into "possible" and "definite." All the spectra were also analyzed using the FXCOR routine in IRAF. Each object was cross-correlated with three different templates: (*a*) a template made up from the 27 best signal-to-noise ratio (S/N) stars in the data, (*b*) a template made up from three high S/N late-type stars, and (*c*) a template made up from 16 emission-line galaxies (all shifted to their rest frames) in the data. For each spectrum, the correlation with the highest peak was then selected. A reassuringly close match was found between the by-eye classification and velocities and the results from FXCOR. The resulting histogram for velocities was inspected. Apart from four low S/N or hot stars (for which a good template was not constructed), the stellar velocities found by FXCOR had a distribution well represented by a Gaussian with zero mean and an approximate dispersion (σ) of 85 km s^{-1}. We take this to be a reasonable estimate for our radial velocity uncertainties. It was also found that the subjective "possible" category in the by-eye radial velocity measurements matched rather well a cross-correlation peak height less than 0.3 returned by FXCOR. Apart from one outlier, the difference between the FXCOR velocity and that measured by eye for the galaxy identifications with cross correlation peak heights above 0.3 also was fairly well fitted by a Gaussian with $\sigma = 85$ km s^{-1}.

In the end we obtained 129 definite galaxies, 43 possible galaxies, 86 definite stars, four possible stars, 10 fibers that had to be unplugged due to overillumination (which were hence almost certainly stars), 37 fibers which showed no flux (either very low surface brightness galaxies or positional errors), and 21 spectra which showed flux but which were unclassifiable as either stars or galaxies (based on very low cross-correlation peak heights from FXCOR and visual inspection). We should reiterate that a much higher "success" rate in finding galaxies could have been achieved by raising the cutoff "sigma" value used in choosing galaxies from the APM scans, at the cost of missing some compact galaxies.

We present in Table 1 the resulting galaxy redshifts. For each object, the table lists the right ascension and declination, an approximate *B*-magnitude, and the heliocentric radial velocity. The magnitudes were calculated using the APM isophotal magnitudes measured from the plates, crudely calibrated using the *B*-magnitudes listed by Stockton (1980) and Salzer (1992) for objects in the scanned region. They could be in error by as much as 0.5.

A number of the brightest galaxies in the field were not included in the fiber survey. Those with known redshifts within the survey region were added to the sample (four objects taken from the 1990 May 5 version of the CfA Redshift Catalog [Huchra 1990]). This gives a total sample of 176 galaxies with redshifts within the survey region, which is roughly complete to a *B*-magnitude of 19.0.

We plot the results of the survey in a number of projections. Figure 3 shows a redshift histogram of the galaxies, Figure 4 shows the distribution of galaxies on the sky, while Figure 5 shows the pie diagrams obtained.

3. ANALYSIS

In this section we go through each of the three observations described in § 2 in turn, deriving constraints on the absorbers. In § 3.1 we derive limits on Hα line emission at the velocities of the narrow-band filters, and in § 3.2 we calculate the maximum

© American Astronomical Society • Provided by the NASA Astrophysics Data System

1993ApJ...419..524M

TABLE 1

GALAXY REDSHIFTS IN 3C 273 FIELD

RA(1950)	Dec(1950)	B[a]	z(Hel.)	RA(1950)	Dec(1950)	B[a]	z(Hel.)	RA(1950)	Dec(1950)	B[a]	z(Hel.)
Definite Redshifts											
12:22:08.84	2:07:34.8	17.19	0.04426	12:26:08.06	2:46:36.8	18.61	0.15898	12:29:55.23	2:25:15.6	18.98	0.10089
12:22:29.45	2:47:19.0	18.58	0.07701	12:26:13.59	2:20:24.1	18.79	0.17770	12:29:57.28	2:23:24.2	18.74	0.08072
12:22:30.88	2:05:29.9	18.45	0.07485	12:26:18.41	2:22:37.3	18.34	0.09010	12:30:02.98	1:46:40.6	18.57	0.07915
12:22:33.22	2:00:15.8	18.08	0.08985	12:26:36.82	2:06:38.4	17.67	0.07779	12:30:03.25	2:35:24.7	17.72	0.07557
12:22:37.94	1:47:01.0	18.19	0.07994	12:26:38.63	1:53:05.5	17.85	0.15652	12:30:09.78	2:47:59.0	18.12	0.07982
12:22:40.70	2:49:34.3	17.99	0.06892	12:26:39.99	2:29:27.8	18.07	0.07743	12:30:17.93	2:54:15.6	17.31	0.00595
12:23:01.21	2:04:24.4	18.24	0.08969	12:26:46.20	2:01:11.7	18.89	0.16438	12:30:22.94	2:39:13.8	18.55	0.07568
12:23:07.24	2:38:12.6	17.10	0.04999	12:26:47.59	2:44:25.4	18.51	0.13946	12:30:27.96	2:36:36.4	17.59	0.07703
12:23:09.52	2:17:02.1	18.70	0.17614	12:26:50.65	2:24:46.1	18.23	0.14668	12:30:36.80	2:35:10.3	18.21	0.07957
12:23:11.47	1:50:43.1	16.89	0.07956	12:26:51.27	2:26:14.7	18.95	0.07789	12:30:37.24	2:51:01.0	18.30	0.12286
12:23:17.05	1:43:11.2	18.20	0.02353	12:26:52.38	1:36:55.3	18.31	0.15554	12:30:42.62	2:30:57.6	18.68	0.08120
12:23:30.44	2:33:35.7	18.82	0.07646	12:26:52.52	1:39:47.2	18.09	0.09756	12:30:47.21	1:47:53.7	15.51	0.00613
12:23:32.93	2:50:24.6	18.21	0.09982	12:26:57.40	1:56:31.8	18.83	0.13388	12:30:49.66	2:25:19.1	18.77	0.07982
12:23:46.18	2:00:03.5	16.96	0.02340	12:27:02.59	2:46:31.9	17.59	0.03022	Possible Redshifts			
12:23:55.39	2:01:13.3	18.86	0.16096	12:27:03.63	2:46:39.3	19.12	0.03057				
12:23:57.61	2:08:48.8	18.89	0.07713	12:27:07.80	2:07:30.3	19.09	0.07788	12:22:07.58	2:46:59.4	18.00	0.10029
12:24:03.62	1:56:06.2	18.17	0.07802	12:27:15.67	2:17:27.6	18.15	0.15834	12:22:08.45	2:31:20.8	18.52	0.13555
12:24:16.04	1:51:00.7	16.92	0.08933	12:27:20.02	2:32:37.5	17.93	0.02776	12:22:13.42	2:35:04.8	18.58	0.13823
12:24:19.04	1:45:03.9	18.19	0.13047	12:27:24.33	1:59:14.4	18.49	0.10450	12:22:22.66	2:50:41.0	18.10	0.09076
12:24:23.43	2:25:30.6	18.85	0.17566	12:27:36.64	2:20:12.3	19.10	0.10343	12:22:29.27	2:04:15.4	17.95	0.02273
12:24:30.49	2:06:43.3	18.71	0.08122	12:27:39.39	1:54:16.7	18.10	0.07523	12:22:30.77	2:35:32.7	18.86	0.13511
12:24:31.48	2:11:48.6	18.77	0.18785	12:27:40.60	2:36:31.4	17.90	0.07991	12:22:31.91	1:57:18.2	18.78	0.07145
12:24:31.61	2:13:19.9	18.83	0.15703	12:27:40.96	2:34:04.0	18.56	0.07931	12:22:33.88	2:08:05.4	18.97	0.16052
12:24:32.42	2:30:34.7	18.57	0.17514	12:27:41.56	2:31:31.0	18.01	0.10316	12:22:56.09	2:26:50.6	18.79	0.13350
12:24:33.75	1:59:48.8	18.57	0.04375	12:27:57.12	2:34:24.1	18.22	0.15762	12:23:03.55	2:11:55.1	18.65	0.06375
12:24:35.02	2:16:16.5	17.46	0.08820	12:27:59.76	1:44:49.0	17.69	0.03096	12:23:16.57	1:41:16.4	18.43	0.17263
12:24:38.46	2:30:37.5	18.45	0.04957	12:28:00.72	2:22:29.5	18.95	0.19400	12:23:38.97	2:34:36.8	18.56	0.15820
12:24:40.59	2:59:40.6	18.59	0.13905	12:28:01.20	2:18:42.2	18.82	0.15758	12:23:50.85	1:56:56.6	18.83	0.21653
12:24:42.57	2:07:39.3	18.26	0.07827	12:28:01.89	1:46:43.9	19.13	0.03061	12:24:19.95	2:56:10.5	18.29	0.08590
12:24:43.73	2:49:18.2	18.44	0.13807	12:28:04.97	1:38:25.9	18.76	0.12065	12:24:20.67	2:33:40.0	18.44	0.13823
12:24:46.30	2:57:45.9	18.34	0.07814	12:28:14.83	2:40:08.0	18.64	0.07601	12:24:27.79	1:40:48.9	18.98	0.13268
12:24:46.37	3:05:35.8	18.42	0.08047	12:28:17.51	1:55:11.7	18.83	0.02531	12:24:36.86	3:03:50.4	18.91	0.08564
12:24:47.11	3:00:19.0	17.42	0.07970	12:28:19.36	2:05:48.6	18.55	0.02533	12:24:44.24	2:52:41.0	19.10	0.21953
12:24:55.75	1:44:20.9	18.78	0.11983	12:28:19.98	2:14:47.6	18.24	0.10265	12:24:45.97	2:17:16.6	17.83	0.08844
12:25:04.64	2:11:41.8	18.45	0.07823	12:28:21.93	2:28:14.4	18.00	0.15701	12:24:48.59	1:41:13.1	18.54	0.15585
12:25:12.50	2:12:50.6	18.82	0.09251	12:28:22.11	1:59:19.4	18.57	0.07855	12:25:17.59	1:41:32.9	18.48	0.07970
12:25:17.26	1:36:48.8	18.71	0.10056	12:28:22.71	1:46:47.3	17.96	0.07990	12:25:36.43	3:01:49.8	19.02	0.08672
12:25:19.87	2:07:59.8	18.14	0.09266	12:28:24.14	1:59:23.5	17.55	0.07862	12:25:39.61	1:41:41.6	18.68	0.11054
12:25:19.92	1:58:51.4	18.43	0.13821	12:28:40.19	1:47:21.4	17.52	0.02539	12:25:47.83	2:31:42.1	19.02	0.15380
12:25:26.17	2:42:24.2	17.73	0.11790	12:28:41.38	1:48:23.1	18.66	0.12109	12:26:02.26	1:47:58.0	18.71	0.09276
12:25:28.11	1:53:04.4	17.23	0.07710	12:28:45.15	3:02:41.5	18.47	0.09946	12:26:13.45	1:42:02.7	19.06	0.11949
12:25:35.24	1:54:36.8	18.48	0.07746	12:28:50.36	1:58:08.2	18.31	0.07328	12:26:29.41	2:36:18.3	19.10	0.15616
12:25:37.98	1:53:39.2	18.61	0.07752	12:28:57.09	3:01:32.4	17.09	0.02949	12:26:58.82	2:10:38.7	18.97	0.17319
12:25:38.87	1:53:51.6	18.29	0.07689	12:29:03.70	2:03:55.5	18.14	0.14173	12:27:01.55	1:40:23.0	18.22	0.08870
12:25:42.50	2:58:37.6	16.31	0.00777	12:29:08.26	1:49:17.2	17.87	0.08818	12:27:02.89	2:06:27.1	19.10	0.07703
12:25:43.43	2:36:53.4	18.88	0.15727	12:29:11.20	2:02:22.6	18.54	0.14154	12:27:03.93	2:53:05.9	17.88	0.10048
12:25:44.35	2:29:03.5	18.98	0.12067	12:29:15.41	2:26:44.1	18.47	0.21553	12:27:13.78	2:10:37.1	19.07	0.15482
12:25:46.88	2:25:48.5	17.34	0.15841	12:29:19.03	2:32:43.7	18.79	0.07959	12:27:28.01	2:01:39.1	18.96	0.18136
12:25:47.43	2:38:09.1	18.58	0.08766	12:29:19.14	2:59:17.5	18.31	0.08088	12:27:40.40	2:54:03.2	15.25	0.00616
12:25:49.80	2:25:49.8	17.90	0.15738	12:29:22.90	2:15:05.5	18.88	0.07514	12:28:00.33	2:01:40.0	18.58	0.07966
12:25:53.78	2:19:24.5	18.30	0.15909	12:29:25.42	1:41:48.4	18.42	0.13500	12:28:05.06	2:51:22.3	17.95	0.10308
12:25:55.11	2:27:43.9	18.62	0.08798	12:29:32.77	1:40:49.2	17.76	0.07664	12:28:19.91	2:27:39.8	18.97	0.15911
12:25:56.93	2:23:05.2	17.31	0.03253	12:29:39.04	2:12:14.2	18.66	0.20746	12:29:16.89	1:39:37.9	17.92	0.16278
12:25:58.11	2:15:41.3	18.37	0.15878	12:29:42.32	2:50:24.6	18.34	0.07774	12:29:19.25	2:05:19.8	18.38	0.07884
12:25:58.55	2:44:08.6	18.27	0.15793	12:29:43.62	2:37:49.3	18.17	0.07564	12:29:23.16	2:31:05.5	18.93	0.12068
12:26:00.95	2:04:50.3	17.95	0.09225	12:29:47.33	2:29:29.6	18.88	0.08091	12:30:23.08	2:51:07.3	18.95	0.08164
12:26:03.90	2:55:03.2	18.00	0.07792	12:29:48.77	1:54:33.8	18.96	0.18496	12:30:24.87	1:49:03.0	18.23	0.07658
12:26:06.69	2:11:01.3	18.08	0.02938	12:29:52.29	2:22:27.3	18.88	0.06301	12:30:31.73	2:13:03.3	18.51	0.08166

[a] See text for discussion of magnitude estimates.

© American Astronomical Society • Provided by the NASA Astrophysics Data System

1993ApJ...419..524M

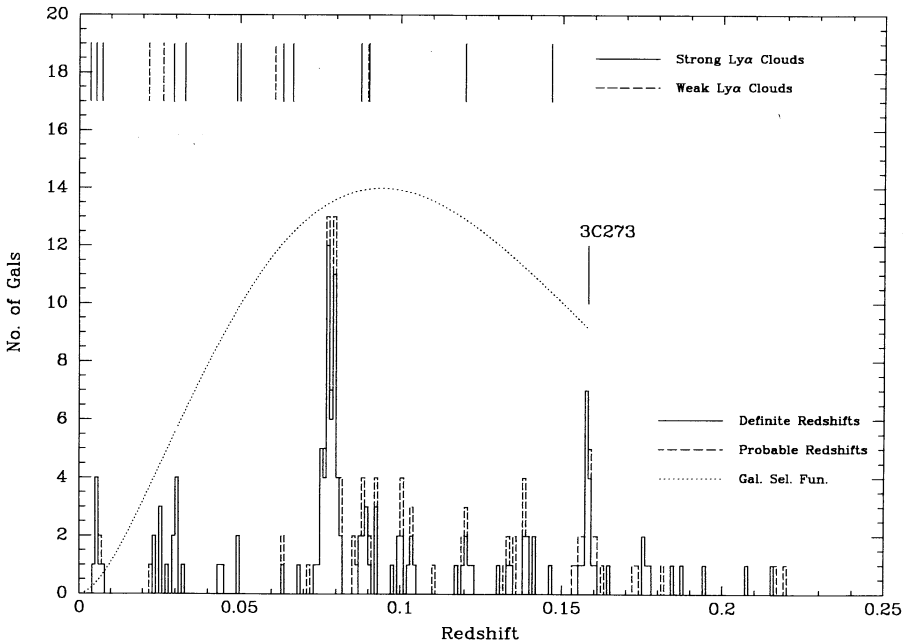

FIG. 3.—Histogram of redshifts of galaxies found in the 3C 273 sight line. Also plotted are the locations of Lyα absorbers from Table 3 (where " strong " refers to lines with EW ≥ 55 mÅ, and " weak " refers to the remainder) and the (arbitrarily normalized) galaxy selection function for the fiber survey. See text, § 2.3.

absolute magnitude a dwarf galaxy could have and remain undetected in our broad-band imaging. A long description of the correlation analysis between the Lyα absorbers and the galaxies found in the fiber survey is given in § 3.3, in which the various available absorber and galaxy subsamples are discussed, and two alternative extreme hypotheses for the absorber-galaxy correlation function are tested. Finally, in § 3.4 we discuss some particular aspects of the absorber-galaxy distribution found in the 3C 273 sight line.

3.1. *Flux Limits for* Hα *Line Emission*

The final continuum-subtracted coronagraph images have a measured rms dispersion (away from residuals due to bright stars) of 0.0018 DN pixel^{-1} s^{-1}. From calibration observations of HD 84937, this is equivalent to a 1 σ flux limit of 2×10^{-18} ergs cm^{-2} s^{-1} arcsec^{-2}, equivalent to an emission measure of approximately 2.8 pc cm^{-6}. By blinking the images, it can be seen that none of the objects visible in the broad-band images have emission line fluxes greater than 3 σ. For comparison, the VN2 image of Mrk 49 showed a peak Hα line flux of 3×10^{-14} ergs cm^{-2} s^{-1} arcsec^{-2}, i.e., 5000 times higher than our 3 σ detection limit. One can also perform the following thought experiment. What would the Orion Nebula look like if placed at the distance of the Virgo Cluster? As discussed in Kennicutt (1984), the Orion Nebula is actually a relatively low-luminosity H II region, with an Hα luminosity of only 10^{37} ergs s^{-1}. Nevertheless, if placed at a distance of 16 Mpc, it would still have a flux of 1.3×10^{-15} ergs cm^{-2} s^{-1} (and would be unresolved—the nebula has a diameter of 5 pc, while at Virgo 1″ corresponds to approximately 80 pc). Thus it would be a factor of 220 brighter than our 3 σ limit. One can also calculate that the Strömgren sphere around a single main-sequence star of spectral class ~B1 per square arcsecond would be detectable at the 3 σ level (Allen 1973, p. 267).

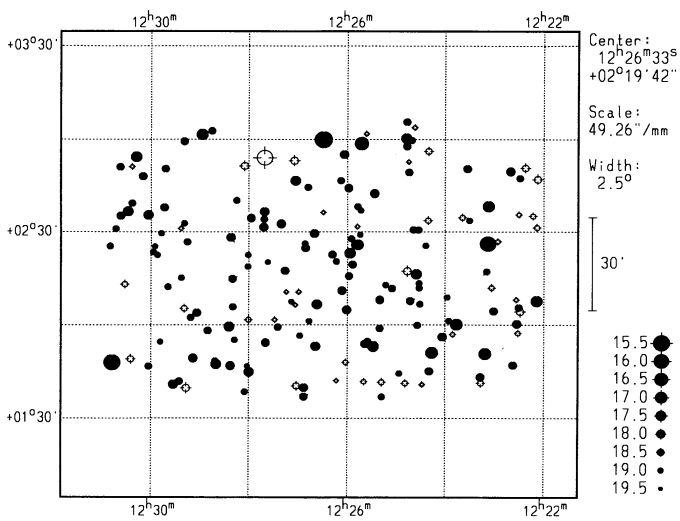

FIG. 4.—Locations on the sky of the galaxies with redshifts in the field of 3C 273. See text, § 2.3.

Unfortunately, the expected surface brightness of an optically thick slab of hydrogen, simply bathed in the local UV background, would not be detectable. Taking the limit on the UV background from Songaila, Bryant, & Cowie (1989), and using the formulae from Osterbrock (1989), one finds a surface brightness of $\lesssim 3 \times 10^{-19}$ ergs cm^{-2} s^{-1} arcsec^{-2}, about a factor of 20 below our 3 σ limit.

Higher spectral and spatial resolution data have been taken by T. Williams (1993, private communication) using the Rutgers Fabry-Perot system at the CTIO 4 m telescope. These data have not been fully analyzed, but they should produce even lower surface brightness limits (or detection) than our data.

3.2. *Limiting Magnitude for Detection of Low Surface Brightness Dwarf Galaxies*

The main motivation for taking the COSMIC images was to determine whether there were any dwarf galaxies within a 40

© American Astronomical Society • Provided by the NASA Astrophysics Data System

1993ApJ...419..524M

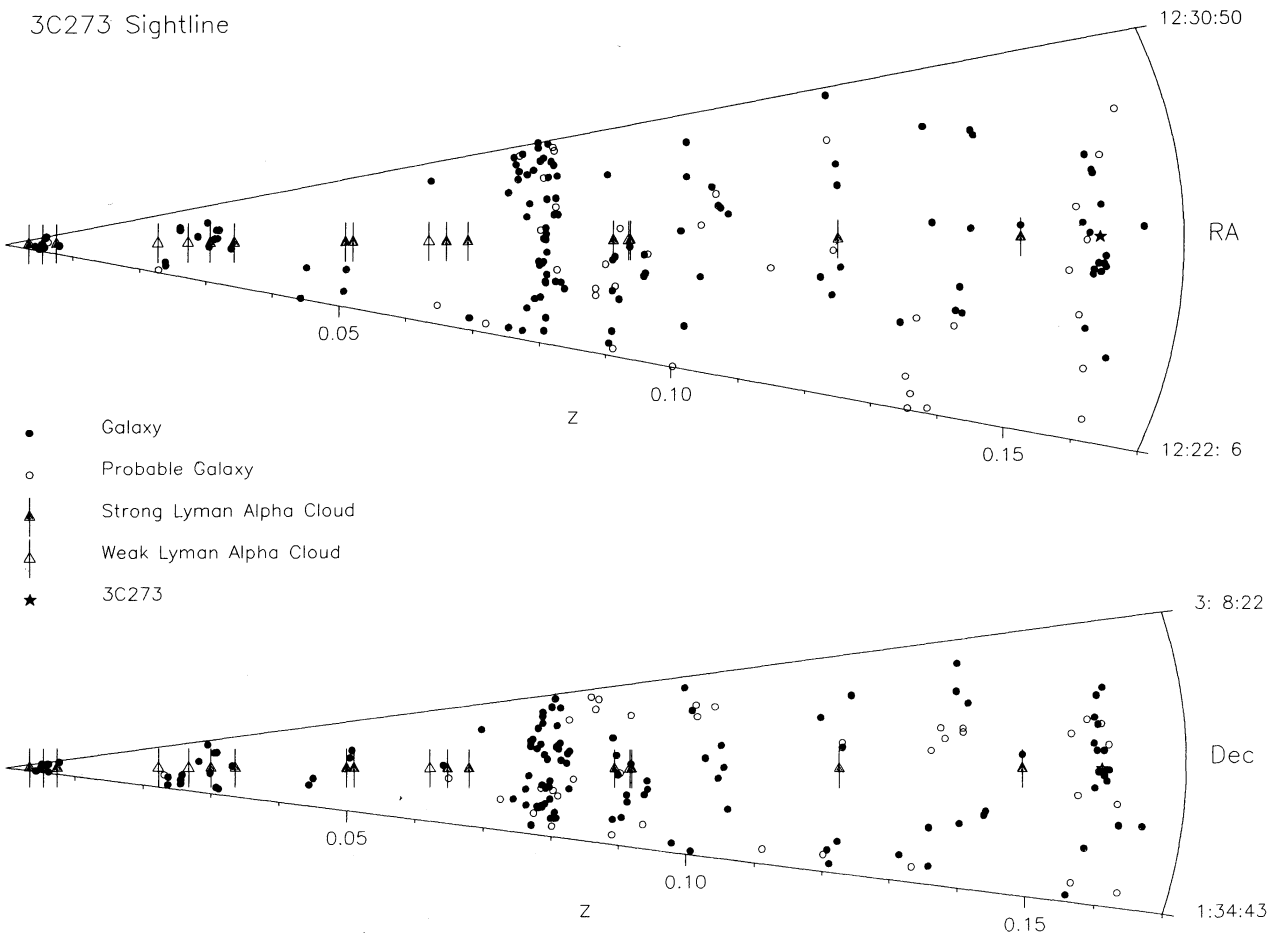

FIG. 5.—Pie diagrams of the galaxies observed with the LCO fiber system. Angles have been exaggerated by a factor of 15 to prevent overcrowding of the symbols. Please note that this results in a highly distorted plot with initially spherical structures (such as the 3C 273 cluster of galaxies) appearing elongated transverse to the line of sight. Note also that the star marking the position of 3C 273, while readily visible in the projection in right ascension, is partially obscured by a clump of galaxies in the projection in declination.

kpc radius from the line of sight to 3C 273 which are too faint to be visible on the POSS plates. Examples of low surface brightness dwarfs in the Virgo Cluster can be seen in Sandage & Binggeli (1984). In order to determine how faint a dwarf galaxy, which had morphological properties typical of those found in the Virgo Cluster, would be detectable in our image, we used the IRAF ARTDATA package to insert artificial dwarf galaxies into the data array. The magnitude scale was derived by assuming that the sky background in the Gunn r band (before the Moon rose) was 21.5 (Massey 1990). B absolute magnitudes were converted to Gunn r assuming a $B-R$ color of 1.0 ($B-V$ of 0.7), and a conversion from R to Gunn r of $r = R+0.43+0.15(B-V)$ (Kent 1985). Thus a dwarf galaxy with $M_B = -15.5$ was taken to have $M_r = -16.0$. The Virgo distance modulus was taken to be 31.02. Dwarf galaxy properties were taken from Binggeli et al. (1985). In particular, typical exponential scale lengths[4] for Virgo dwarfs were taken to be 2–4 kpc. Figure 6 shows the same data as Figure 2, but with three dwarf galaxies added. One to the northeast with $M_B = -14.5$ and scale length 4.4 kpc, one to the northwest with $M_B = -13.5$ and scale length 2.2 kpc, and one to the southwest with $M_B = -13.5$ and scale length 4.4 kpc. These experiments demonstrated that we would be able to detect dwarf galaxies as faint as -13.5 at the distance of Virgo, having morphological properties similar to those found near the cluster center. For comparison, the dwarf galaxy illustrated in Figure 2 of Sandage & Binggeli (1984) (panel 4, labeled "15°47") has an absolute B-magnitude of -14.8.

A complementary approach is to search for H I 21 cm emission from Virgo dwarf galaxies. Recently, van Gorkom and her collaborators have set extremely low limits with the VLA over a 40′ × 40′ field centered on 3C 273 and over a velocity range of about 1000 km s^{-1} centered on 1300 km s^{-1} to a 1 σ column density limit of approximately 10^{19} cm^{-2} (van Gorkom 1993; van Gorkom et al. 1993).

3.3. *Corrections between Lyman-α Absorbers and Galaxies*

We have shown there are no H II regions, or other strong Hα line-emitting gas, or dwarf galaxies near the Virgo absorbers. Having determined the redshift distribution of galaxies near the sight line to 3C 273 (§ 2.3), we would now like to address the statistical question of the degree to which the Lyα absorbers are correlated with galaxies. If they are correlated, is the Lyα absorber-galaxy correlation the same as the galaxy-galaxy correlation? A cursory inspection of Figure 5 is enough to show that there will not be a simple answer to this question. While there do seem to be Lyα absorbers associated with clumps of galaxies (e.g., the Virgo absorbers, or the set of

[4] Scale length = R_0, with intensity $\propto \exp(-1.6783 \times R/R_0)$.

© American Astronomical Society • Provided by the NASA Astrophysics Data System

1993ApJ...419..524M

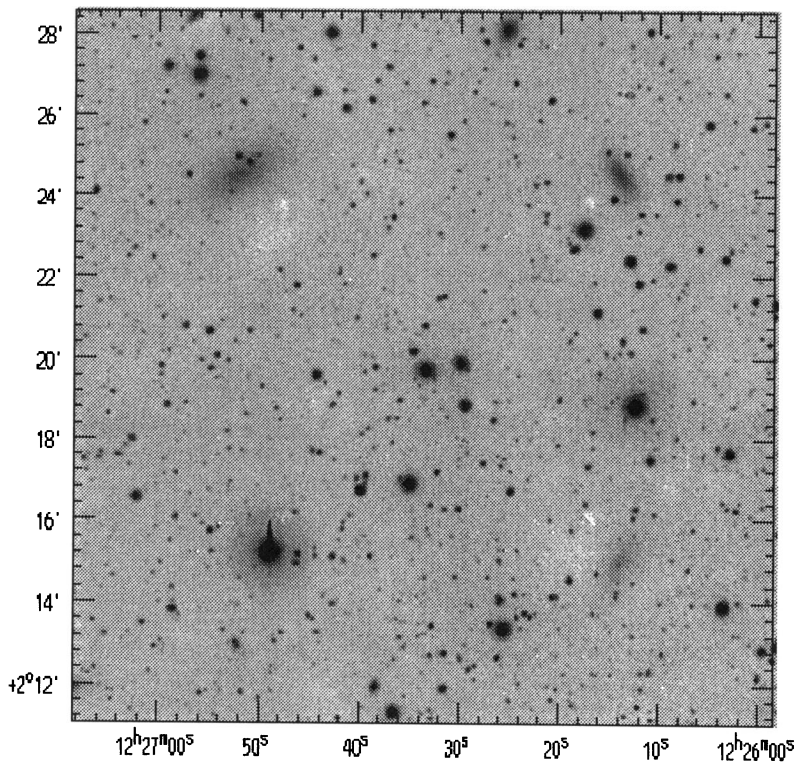

FIG. 6.—Mosaic of COSMIC images in Gunn r of 3C 273 field, with three artificial dwarf galaxies added. Northeast with $M_B = -14.5$ and scale length 15 kpc; northwest with $M_B = -13.5$ and scale length 7.5 kpc, and southwest with $M_B = -13.5$ and scale length 15 kpc. See text, § 3.2.

absorbers around $z = 0.02$–0.03), there are also absorbers in conspicuous "voids" (at $z = 0.06$–0.07), and there are no absorbers associated with the prominent excess of galaxies at $z = 0.078$. We consider statistical tests for various assumptions about the correlation between the Lyα absorbers and the galaxies near the sight line toward 3C 273 for which we have redshift information. Ultimately, the goal should be a quantitative and complete statistical description of the clustering properties of the Lyα absorbers themselves and their correlation with various types of galaxies, clusters, voids, etc. Given both our rather meager understanding of this problem and the small data set, we shall concentrate on testing the following two extreme null hypotheses about the Lyα absorber clustering properties:

1. The Lyα absorbers are uncorrelated with galaxies and are randomly distributed. (The second part of this assumption necessarily implies the first, but the converse is not necessarily true: the absorbers could be correlated among themselves but be uncorrelated with galaxies.)
2. The Lyα absorbers are correlated with galaxies in the same way that galaxies are correlated. More precise formulations of this hypothesis depend upon the particular test applied, as described below.

In carrying out most of the tests described below, it is necessary to compute the three-dimensional distance between every absorber-galaxy or every galaxy-galaxy pair. The question arises as to how to compute the component along the line of sight, since departures from a perfectly smooth Hubble flow distort the mapping of redshift onto radial distance. With no information other than the angular coordinates and redshifts for the objects, we cannot uniquely determine the separation along the line of sight for any individual pair of objects. For purposes of statistical tests we therefore make two different assumptions about this component; the degree to which we do or do not derive similar results will provide some indication of the sensitivity of the test to the uncertainty in the estimation of this component:

1. We simply ignore any departures from Hubble flow.
2. We adopt the formalism of Davis & Peebles (1983) to estimate this component. These authors show how, knowing the two-point correlation function for the *projected* distance between pairs, in principle one can invert the integral equation relating the projected distance correlation function to the three-dimensional spatial correlation function. However, for our limited and rather noisy sample, this is not a very satisfactory procedure. Moreover, we would like statistical estimates for the three-dimensional separation for each pair for the purposes of carrying out other types of tests (e.g., nearest-neighbor tests). We therefore use the Davis-Peebles formalism as follows: adopting the assumptions described in their paper, the integrand in their equation (22) represents the probability that a pair with projected separation r_p Mpc and velocity difference π km s^{-1} has a separation in the radial direction of y Mpc. We further assume their function form for $h(r)$ in their equation (23), with the parameter $F = 1$, and adopt their functional form for $f(V)$, the probability of the relative velocity difference, as well as their expression for σ, the dispersion in $f(V)$, i.e., their equation (32). For $r_p \gg r_0$ or $\pi \gg H_0 r_0$, where r_0 is the characteristic correlation length, the probability is strongly peaked at $y \sim H_0 \pi$, i.e., the pair separation is very likely to be that given by assuming a pure Hubble flow. However, as both of these inequalities fail to be satisfied, a second maximum in the prob-

© American Astronomical Society • Provided by the NASA Astrophysics Data System

1993ApJ...419..524M

ability distribution arises at $y = 0$ whose height depends upon the strength of the correlation—i.e., a pair with a moderate velocity separation and small projected separation may be separated by their Hubble flow distance, but if the correlation between such pairs is strong, this moderate velocity separation is more likely to arise from a pair at about the same distance from us, with strong gravitational interaction between them. As noted at the outset of this discussion, there is no way to determine the relative separation of any pair along the line of sight unambiguously, but since we are interested in statistical applications, *we adopt the expectation value of this probability distribution as our second alternative algorithm.*

A problem with this second approach is that evaluating the probability distribution for the radial separation of the pair requires that we know in advance the two-point correlation function between the pair. Ideally, we could have dealt with this problem by using an iterative approach: for both the absorber-galaxy and galaxy-galaxy pairs separately, we start with some "fiducial estimates" for the two-point correlation (e.g., $r_0 = 5.4\ h^{-1}$ Mpc and $\gamma = 1.77$; cf. eq. [19] in Davis & Peebles 1983) to compute the expectation value of the radial separation for each pair, and thus compute the two-point correlation functions. With these new, separate best-fit values of γ and r_0 for the correlation functions for the galaxy-absorber pairs and the galaxy-galaxy pairs, we could then repeat the process until the parameters for the two-point correlation functions have converged. In fact, since the results of our statistical tests do not appear to be very sensitive to departures from a pure Hubble flow, we have not carried out this iteration but have simply used the single set of parameters ($r_0 = 5.4\ h^{-1}$ Mpc and $\gamma = 1.77$) in calculating the expectation values for both sets of pairs.

In the following, we refer to these two algorithms for estimating the radial separations as the "pure Hubble flow" and "perturbed Hubble flow" cases. When listing object separations in the following sections, we will give the separations found from the expectation value of the perturbed Hubble flow model in parentheses following the value for the pure Hubble flow model.

Before carrying out any statistical tests, we define the two samples and discuss appropriate corrections for completeness.

3.3.1. *The Lyman-α Sample*

A carefully defined list of Lyα absorption lines is essential to a proper statistical discussion of the correlation properties of Lyα absorbers with galaxies. The preferred list would obviously be drawn from a homogeneous set of observations with the smallest detectable equivalent width covering all or most of the relevant redshift range.

Several line lists for the 3C 273 sight line have been published (Morris et al. 1991; Bahcall et al. 1991a, b; Brandt et al. 1993; Bahcall et al. 1993). These line lists are compared in Table 2. However, not only are these lists based upon three different *Hubble Space Telescope* (*HST*) spectrograph configurations (GHRS G160M, GHRS G140L, FOS G130) but they have also been produced by different reduction procedures and line-finding and line-measuring algorithms and with differing acceptance criteria for what constitutes a "real" line. To investigate the importance of this latter source of inhomogeneity, we have run the same continuum fitting, absorption line-finding and line-measuring software, JASON, used for the FOS line

TABLE 2

COMPARISON OF 3C 273 EXTRAGALACTIC ABSORPTION LINE LISTS

Morris *et al.* 1991		Brandt *et al.* 1993			Bahcall *et al.* 1991b		Bahcall *et al.* 1993		Sample[b] &
λ (Å)	EW (mÅ)	λ (Å)	EW (mÅ)	Sig. Lev.[a]	λ (Å)	EW (mÅ)	λ (Å)	EW (mÅ)	Comments
1220.00	-	1219.19	130	6.7	1219.80	371	1219.74	470	T [c]
1222.20	-	1222.31	157	10.1	1222.12	414	1222.04	420	T [c]
-	-	-	-	< 3	1224.52	240	-	-	T [cd]
1242.17	27	-	-	3.2	-	-	-	-	TH [e]
1247.54	32	1247.49	61	4.8	-	-	-	-	TH [e]
1251.46	120	1251.46	120	9.9	-	-	-	-	THS
1255.70	74	1255.44	65	4.9	-	-	-	-	THS
1275.19	144	1275.19	139	10.9	1275.23	251	1275.01	180	THS
1276.54	68	-	-	< 3	-	-	-	-	THS [f]
1289.79	52	-	-	3.4	-	-	-	-	TH [e]
1292.84	63	1292.73	48	5.4	-	-	-	-	THS
1296.57	302	1296.46	324	24.0	1296.52	287	1296.46	320	THS
-	-	-	-	-	1317.08	292	-	-	- [g]
1322.16	75	1322.04	60	4.6	-	-	-	-	THS
1324.96	27	1324.91	143	7.7	1325.10	238	1324.98	210	TH [e]
1325.22	57	-	-	8.1	-	-	-	-	THS [h]
1361.63	126	1361.63	133	12.4	1361.53	146	-	-	THS
1393.86	331	-	-	-	-	-	-	-	THS [i]

[a] Significance level from Key Project JASON software; see text.
[b] Lyα sample membership: T = total, H = homogeneous, S = strong; see text.
[c] Outside wavelength range covered by GHRS high-dispersion data.
[d] Possibly seen in GHRS G140L data. Not listed in Bahcall et al. 1991b, but given in Bahcall et al. 1991a.
[e] GHRS marginal detection according to Morris et al. 1991.
[f] Line not found in re-reduced GHRS data; JASON significance level = 4.5 in original GHRS reduction. See text.
[g] Possibly Ni II; see text and Brandt et al. 1993 for discussion.
[h] Blended with line above in Brandt et al. 1993 and FOS data.
[i] Blended with Si IV; see text and Morris et al. 1991 for discussion.

© American Astronomical Society • Provided by the NASA Astrophysics Data System

1993ApJ...419..524M

list, which is described in detail by Schneider et al. (1993)[5] on the data sets of Morris et al. (1991) and Brandt et al. (1993). The JASON software was designed to run on FOS data with an approximately Gaussian point spread function (PSF). Unfortunately, this is not a good representation for the GHRS large-aperture PSF, and also in general the lines were resolved—meaning that the observed line profiles had neither the instrumental PSF nor a Gaussian shape. The current version of JASON does not perform such convolutions, and so we have run the search routines assuming a fixed PSF with the correct (non-Gaussian) shape for the GHRS, but with no account taken of resolved lines. This means that the equivalent widths (EWs) output by the JASON software are not accurate, but the detection significance levels are approximately correct (see Schneider et al. 1993). The data set used is that described by Brandt et al. (1993). We tabulate the significance levels from JASON for the Lyα lines in column five of Table 2, after the positions and EWs published in Brandt et al. (1993). It can be seen that all of the "reliable" lines listed by Morris et al. (1991) are confirmed by the JASON software, with the notable exception of the line at 1276.54 Å, which was also not found by Brandt et al. (1993). We checked this line by running the JASON software on the original data used by Morris et al. (1991), obtaining a significance level of 4.5 for the line. The line-finding and line-fitting software used in Morris et al. (1991) was developed by R. Carswell and J. Webb and is described in that paper. It used the GHRS PSF convolved with a Voit profile with variable width.

Two other entries in Table 2 require special comment. First, the line at $\lambda = 1317.08$ Å is identified as Lyα in the list of Bahcall et al. (1991b), whereas in the list of Morris et al. (1991) it is identified as Ni II. This issue has been discussed in detail in Brandt et al. (1993), who give reasons for preferring the Ni II identification which we adopt. The second case involves the line at $\lambda = 1393.86$ Å. As discussed in detail by Savage et al. (1993), this line appears to be a blend of one of the members of the Galactic Si IV doublet and another strong line, whose only plausible identification is Lyα. The procedure used by Morris et al. (1991) in estimating the strength of this line (which involves a detailed comparison of the line profiles of the Si IV doublet) is not incorporated into the JASON formalism. For this reason we cannot assign a formal uncertainty in the line strength. However, the residuals from an unblended fit to the Si IV doublet are highly significant.

As a result of the above considerations, we have decided to adopt the following samples of absorbers for our statistical tests: (1) For the Lyα absorber "*total* sample" we adopt the list of 16 Lyα absorbers (and their redshifts) given in Morris et al. (1991) along with the additional low-redshift line (λ1224.52) given by Bahcall et al. (1991a); as noted in Table 2, this last line is visible in the GHRS G140L spectra but was below the significance threshold of Morris et al. (1991). This "total sample" is inhomogeneous and/or biased in three senses: (i) The high-resolution GHRS data covers only redshifts above $z \sim 0.016$; below this, only the Faint Object Spectrograph (FOS) data of Bahcall et al. (1991b) and the GHRS G140L low-resolution data are available. (Observations with the GHRS G160M grating in the redshift regime from 0.0 to 0.016 are scheduled for *HST* Cycle 3.) Thus, the total sample may be biased against weak low-redshift lines in this redshift range that may be detected by these Cycle 3 observations. (ii) The line of sight toward 3C 273 may be somewhat atypical in that it passes through the southern extension of the Virgo Cluster. (iii) Some of the weakest lines listed as "possible" in the Morris et al. (1991) list may not be real. Accordingly, along with the full sample of 17 lines, we shall also consider two subsamples: (2) A "*homogeneous* sample" made of the set of 14 lines found only with the GHRS G160M observations using the original Carswell and Webb software (i.e., all but the first three lines in col. [1] of Table 2). (As it happens, this is also equivalent to detecting the three low-redshift ($z \lesssim 0.016$) lines possibly associated with the Virgo Cluster.) (3) A "*strong* sample" composed of the set of 10 lines from Morris et al. (1991) with $-\log(P) > 7.5$ (but including the line at $z = 0.14658$ for which a formal probability estimate was not possible due to blending—i.e., the above sample with the lines marked "e" in the "Comments" column of Table 2 removed). We have listed the sample membership in the final column of Table 2. Note that in contrast to the galaxy sample discussed below there is no intrinsic observational selection against the higher redshift absorbers.

One could, of course, define further samples. In particular, at the request of the referee, we have also run our statistical tests of the complete set of five lines listed in Bahcall et al. (1993) (i.e., the line list in col. [8] of Table 2). Unfortunately, the number of lines in this list is so small that neither of the two null hypotheses considered below in connection with cloud-galaxy association can be rejected with any significance. For this reason, and in order to keep the various combinations of absorption-line and galaxy samples to manageable proportions, we limit our tables of statistical results to consideration of the three samples defined above.

3.3.2. *The Galaxy Sample*

An appropriate sample of galaxies with which to carry out the correlation analysis would be one which is complete to some limiting absolute magnitude throughout a cylindrical volume centered on the 3C 273 sight line (i.e., out to a constant impact parameter) with a radius large enough to sample most of the expected power in the correlation function and length over (and beyond) the full redshift range covered by the Lyα line sample. The observed sample described in § 2.3 fails this requirement in two obvious respects: (1) it detects only the more luminous galaxies at the higher redshifts, and (2) it contains no galaxies with large impact parameters at low redshifts. For some tests these deficiencies are probably not important, but for others they are. Accordingly, we will consider two galaxy samples. The first is the sample described in § 2.3, which we will refer to as the "cone" sample. The second is the cone sample together with all galaxies from the 1990 May 5 version of the CfA Redshift Catalog (Huchra 1990) within 10 Mpc of the 3C 273 line of sight. This gives a heterogeneous sample with an unknown selection function, but is closer to the ideal "filled cylinder" than the cone sample. It contains 1498 galaxies, the vast majority being the Virgo distances, and will be referred to as the "cylinder" sample.

Thus, for each hypothesis tested below, there are eight galaxy-absorber sample combinations and two possible estimates for the distance between every pair of objects, giving a total of 16 data sets for each statistical test.

3.3.3. *Tests of the First Null Hypothesis: The Lyman-α Absorbers Are Uncorrelated with Galaxies*

It is obvious that this hypothesis cannot literally be true; every sight line that passes close to any galaxy, except those utterly devoid of gas, will surely produce a detectable Lyα line, and indeed examples of this are already known (Bahcall et al.

[5] We thank D. Schneider for kindly making available the most recent version of JASON and for instruction in its use.

© American Astronomical Society • Provided by the NASA Astrophysics Data System

1993ApJ...419..524M

1992a, b). Nevertheless, in light of the fact that the high-redshift Lyα absorbers show almost no power in their two-point correlation function (cf. Rauch et al. 1992 and references therein), it is of interest to see whether the present data set does or does not exclude this hypothesis and, if it does, how strongly.

Having formulated this null hypothesis, we consider two statistics as measures of correlation (or lack of it):

1. The average over all the Lyα absorbers of the distance between a given Lyα absorber and the N nearest galaxies in the sample, with $N = 1$, 3, and 5.
2. The total number of absorber-galaxy pairs within a fixed radius R, with $R = 500$ kpc and 10 Mpc.

In order to see whether the values of these observed statistics are such that the null hypothesis can be rejected, we must find the distribution of these same statistics for many realizations of the null hypothesis. To do this, we carry out 1000 Monte Carlo simulations in which the same number of absorbers as that of the particular Lyα sample under consideration are laid down randomly [but follow the "global" distribution $dN/dz \sim (1 + z)^{0.3}$ as determined by Bahcall et al. 1993]. Redshift limits for the random absorbers were $0.03 < z < 0.151$ for the total sample and $0.016 < z < 0.151$ for the homogeneous and strong samples.

The results for the nearest-neighbor tests are summarized in Table 3. We show results for the single nearest-neighbor galaxy, the mean of the three nearest, and the mean of the five nearest. For each case, the three columns list the observed mean nearest-neighbor(s) distance, the average of the mean nearest-neighbor(s) distances produced by the Monte Carlo simulations, and the number of the 1000 Monte Carlo simulations that had a mean nearest-neighbor distance less than the observed one. Thus this last column, divided by 1000, can be taken as the probability that the observed value could arise from a sample of absorbers distributed at random with respect to the galaxies.

The most striking result is that there is a less than 0.1% probability that the average nearest-neighbor distance to the single closest galaxy could arise from a randomly distributed set of absorbers. This is true for all sample combinations, and for either pure or perturbed Hubble flow. For all samples, as one includes more galaxies in the nearest-neighbor average, the significance drops. After seeing this result, we wanted to test whether all the significance came from the nearest galaxy, and so ran tests on the second-nearest galaxy only (also given in Table 3). One can see that the observed mean distance is still significantly lower than that expected for a randomly distributed set of absorbers, but this could be explained by a combination of the highly significant correlation with the nearest galaxy and the strong galaxy-galaxy two-point correlation. This point is discussed in some detail by Phillips, Disney, & Davies (1993) in the context of bright galaxies found near quasar Mg II absorbers.

We also give in Table 4 the right ascension, declination, and redshift of the nearest galaxy in the "cylinder" sample to each Lyα absorber of the "total" sample (assuming pure Hubble flow). The final column in this table is the minimum absolute magnitude that could have been detected in the fiber survey. This shows that for one absorber there is no known galaxy with absolute magnitude above -17.8 within nearly 10 Mpc (the same distance for the perturbed Hubble flow model) and that even the nearest absorber-galaxy pair in our sample are separated by 350 kpc (240 kpc). We will return to this in § 3.4.

The results of the number of galaxies within a fixed radius of each absorber are given in Table 5. These tests are essentially a comparison of the integrated two-point correlation function out to the given radius (see Mo et al. 1992 for a discussion of this point). The numbers given in the table are the observed number of absorber-galaxy pairs within the given radius, the average of the number of pairs found in 1000 Monte Carlo simulations with randomly distributed absorbers, and the number of the Monte Carlo simulations with a larger number

TABLE 3

NEAREST-NEIGHBOR MONTE CARLO TESTS

Gal[a]	Abs[b]	Nearest Galaxy			2nd Nearest Galaxy			Nearest 3 Galaxies			Nearest 5 Galaxies		
		$\overline{Obs}$[c]	$\overline{Mont}$[d]	N≤O[e]	$\overline{Obs}$[c]	$\overline{Mont}$[d]	N≤O[e]	$\overline{Obs}$[c]	$\overline{Mont}$[d]	N≤O[e]	$\overline{Obs}$[c]	$\overline{Mont}$[d]	N≤O[e]
Pure Hubble Flow													
cylinder	total	2.59	5.52	0	5.03	8.16	3	5.06	7.78	9	6.29	8.83	37
cylinder	homogeneous	3.00	5.97	0	5.93	8.81	18	5.97	8.41	22	7.46	9.57	76
cylinder	strong	2.63	5.96	0	6.01	8.79	49	5.71	8.40	32	6.82	9.55	61
cone	total	2.79	6.91	0	5.64	9.79	2	5.69	9.51	2	7.33	10.85	17
cone	homogeneous	3.00	6.78	0	6.03	9.55	7	6.22	9.36	10	8.09	10.78	47
cone	strong	2.63	6.76	0	6.01	9.53	18	5.94	9.34	16	7.30	10.76	33
Perturbed Hubble Flow													
cylinder	total	2.26	5.56	0	5.06	8.69	5	5.39	8.24	17	7.32	9.48	87
cylinder	homogeneous	2.66	6.04	0	6.05	9.44	17	6.46	8.96	36	8.79	10.32	195
cylinder	strong	2.44	6.03	0	6.29	9.42	59	6.49	8.95	84	8.68	10.30	237
cone	total	2.27	6.98	0	5.21	10.32	2	5.69	10.02	3	8.03	11.60	30
cone	homogeneous	2.66	6.91	0	6.07	10.21	7	6.69	10.00	12	9.42	11.66	113
cone	strong	2.44	6.89	0	6.29	10.19	23	6.77	9.97	39	9.19	11.64	143

[a] Galaxy sample (see text).
[b] Absorber sample (see text).
[c] Observed mean distance to nearest-neighbor galaxies (Mpc).
[d] Average of 1000 Monte Carlo mean distances to nearest-neighbor galaxies (Mpc).
[e] Number (out of 1000) of Monte Carlo tests with mean distance less than or equal to that observed. Thus the percentage probability of the observed value arising from a randomly distributed set of absorbers is this number divided by 10.

© American Astronomical Society • Provided by the NASA Astrophysics Data System

1993ApJ...419..524M

TABLE 4

NEAREST GALAXIES TO 3C 273 LYMAN-α ABSORBERS

z(abs)	EW(abs) (mÅ)	Sep.[a]	Proj.[b] Dist.	Δv[c]	RA(gal) (1950)	Dec(gal) (1950)	z(gal)	M_{abs}[d]	M_{lim}[e]
0.00340	371	0.91	0.86	20	12:35:15.61	5:38:36.0	0.00333	-17.6	-11.4
0.00531	414	0.35	0.23	20	12:26:29.00	2:59:54.0	0.00524	-16.3	-12.4
0.00728	240	0.86	0.59	-50	12:26:58.99	1:07:03.0	0.00745	-15.2	-13.1
0.02180	27	3.73	1.54	-280	12:22:29.28	2:04:15.4	0.02273	-16.7	-15.4
0.02622	32	3.21	2.56	160	12:21:09.00	1:35:16.0	0.02570	-17.3	-15.8
0.02944	120	0.41	0.35	20	12:26:06.68	2:11:01.3	0.02938	-17.1	-16.1
0.03293	74	1.49	0.34	120	12:25:56.93	2:23:05.2	0.03253	-18.1	-16.3
0.04896	144	2.71	1.62	-180	12:24:38.45	2:30:37.5	0.04957	-17.8	-17.2
0.05007	68	2.42	1.62	150	12:24:38.45	2:30:37.5	0.04957	-17.8	-17.2
0.06097	52	7.92	3.32	-610	12:29:52.30	2:22:27.3	0.06301	-17.9	-17.6
0.06348	63	3.69	3.57	-80	12:23:03.55	2:11:55.1	0.06375	-18.2	-17.7
0.06655	302	9.56	4.75	-710	12:22:40.69	2:49:34.3	0.06892	-19.0	-17.8
0.08760	75	1.74	1.15	-110	12:25:55.09	2:27:43.9	0.08798	-18.9	-18.4
0.08990	27	0.82	0.44	-60	12:26:18.42	2:22:37.3	0.09010	-19.2	-18.4
0.09011	57	0.45	0.44	0	12:26:18.42	2:22:37.3	0.09010	-19.2	-18.5
0.12007	126	2.78	1.91	-180	12:25:44.36	2:29:03.5	0.12067	-19.2	-19.0
0.14658	331	1.05	1.00	-30	12:26:50.64	2:24:46.1	0.14668	-20.3	-19.5

[a] Absorber-galaxy separation assuming pure Hubble flow (Mpc).
[b] Galaxy projected distance to 3C 273 line of sight (Mpc).
[c] Absorber-galaxy velocity difference (km s^{-1}).
[d] Approximate absolute *B*-magnitude of galaxy.
[e] Nominal limiting absolute *B*-magnitude of fiber survey at this redshift.

of pairs than that observed. Thus the final column divided by 1000 is the probability that the observed numbers of pairs or more would arise from a random distribution of absorbers.

Table 5 shows that there is no significant excess of galaxies within volumes of radius 10 Mpc centered on the absorbers compared with a random distribution, apart from the cylinder/total subsample. For this combination there are a large number of pairs between the Virgo absorbers and the many Virgo galaxies in the CfA catalog. This result may be interpreted as saying that it is surprising to find three out of 17 absorbers below $z = 0.008$ (although see § 3.4.3). There is a marginally significant excess of absorber-galaxy pairs within 500 kpc, over that expected for a random distribution of absorbers, although the inclusion of the Virgo velocity range removes the significance of this result. In summary, these tests seem to be consistent with the nearest-neighbor distance results, showing that there is an excess of close pairs of absorbers and galaxies, but that this result vanishes if the averaging is done over several galaxies or large radii.

3.3.4. *Tests of the Second Null Hypothesis: Identical Lyman-α Absorber-Galaxy, Galaxy-Galaxy Correlations*

In order to test this hypothesis, one would like to use the same tests as were used in § 3.3.3. A difficulty arises, however, in generating a large number of Monte Carlo samples. We are loath to compare the observed distributions with simulations involving anything other than the actual observed *galaxy* distribution, since differences between the observations and simulations (based, for example, on *n*-body or other galaxy clustering models) may result simply from inadequacies of such models, and it is not clear how to create simulations of (fake) absorber–(real) galaxy distributions having cross-correlation properties which are the same as the observed galaxy-galaxy correlation properties.

One way to deal with this difficulty is to use a test which does not require the generation of Monte Carlo samples: if the absorbers are distributed in the same way as the galaxies, then, given the pencil-beam nature of the galaxy sample, the redshift distributions of the absorbers and the galaxies should be identical, after correction for differing selection effects in the two samples. Table 6 shows the Kolmogorov-Smirnov (KS) *D*-values and probabilities that the absorber redshift distribution is the same as that of the galaxies, after the galaxy distribution is corrected using the selection function shown in Figure 3. This selection function was derived by assuming a Schechter luminosity function with $M_* = -19.5$ and $\alpha = -0.97$ (Loveday et al. 1992). Because this test requires a known selection function, it can only be run for the "cone" galaxy sample. Also, as it directly compares the redshifts, it does not require any assumptions about pure or perturbed Hubble flow. It can be seen from Table 6 that, when all the absorption lines are included, there is a highly significant difference in the redshift distributions. This significance level becomes marginal when the Virgo absorbers are removed, and vanishes when only strong absorbers beyond Virgo are considered.

Our other test of the hypothesis that the absorbers and galaxies have identical correlation functions uses the observed galaxy sample to generate our Monte Carlo "absorber" sample. For each realization a number of the actual galaxy redshifts were selected at random, and were treated as absorbers on the 3C 273 sight line. The actual algorithm involved selecting at random a number of the observed galaxy redshifts equal to the number in the absorber sample (making no correction for the galaxy selection function, and with no restriction on how close together the chosen galaxies were), and treating these redshifts as if they were measured absorber redshifts on the 3C 273 line of sight. The galaxies which provided these redshifts were removed from the galaxy sample for each test, to avoid an excess of "spurious" pairs.[6] The number of absorber-galaxy pairs within a given radius were determined

[6] In fact, leaving in the galaxies would allow one to model a situation where the absorbers were actually part of the halo of one of the observed galaxies, although some maximum halo size would also have to be imposed to make the simulation realistic. We are investigating this point in more detail, and a paper is in preparation (Mo & Morris 1993).

© American Astronomical Society • Provided by the NASA Astrophysics Data System

1993ApJ...419..524M

TABLE 5

PAIR COUNT MONTE CARLO TESTS USING RANDOM ABSORBERS

Gal	Abs	Npair obs[a]	Npair monte[b]	Nmonte>obs[c]
10 Mpc Pure Hubble Flow				
cylinder	total	1952	516.6	10
cylinder	complete	119	101.0	295
cylinder	strong	60	71.8	599
cone	total	98	80.9	269
cone	complete	78	67.2	308
cone	strong	55	47.5	310
10 Mpc Perturbed Hubble Flow				
cylinder	total	1859	492.2	10
cylinder	complete	113	93.7	280
cylinder	strong	57	66.6	581
cone	total	98	75.4	205
cone	complete	75	61.8	281
cone	strong	52	43.7	292
500 kpc Pure Hubble Flow				
cylinder	total	3	0.352	98
cylinder	complete	2	0.063	28
cylinder	strong	2	0.045	7
cone	total	3	0.221	35
cone	complete	2	0.063	28
cone	strong	2	0.045	7
500 kpc Perturbed Hubble Flow				
cylinder	total	10	1.764	63
cylinder	complete	3	0.230	0
cylinder	strong	3	0.172	0
cone	total	6	1.168	105
cone	complete	3	0.230	0
cone	strong	3	0.172	0

[a] Observed number of absorber-galaxy pairs within radius R (Mpc).

[b] Average of 1000 Monte Carlo numbers of absorber-galaxy pairs within radius R (Mpc).

[c] Number (out of 1000) of Monte Carlo tests with a *larger* number of absorber-galaxy pairs within radius R. Thus the percentage probability of the observed value arising from a randomly distributed set of absorbers in this number divided by 10.

for both the real and 1000 Monte Carlo samples, in an identical manner to the second test in § 3.3.3 above. This procedure should be valid as long as the radius within which the pair counts are being made is significantly larger than the typical distance between the galaxy and the 3C 273 line of sight. Because of this, tests were not run for a 500 kpc radius. The results from these tests are given in Table 7. The columns are the same as for Table 5, except that the final column lists the number of Monte Carlo runs with *fewer* absorber-galaxy pairs than the real sample. Thus this number divided by 1000 is the probability that the absorber could have a correlation function as strong as that between galaxies. As can be seen, the absorber-galaxy correlation function averaged over 10 Mpc is significantly weaker than that between galaxies.

TABLE 6

KS COMPARISON OF z-DISTRIBUTIONS

Galaxy	Absorber	KS D	KS % Probability
Cone.....	Total	0.432	0.35
Cone.....	Homogeneous	0.381	3.44
Cone.....	Strong	0.338	20.3

In summary, the two tests above seem to show that the absorber-galaxy correlation function is significantly weaker than the galaxy-galaxy correlation function over large scales (10 Mpc). Even though there is clear evidence for galaxy-absorber clustering, *there is a significant difference between the strength with which the galaxies are clustered with respect to each other and the strength with which the Lyα absorbers are associated with galaxies.*

Some of the results of the two preceding sections can be inferred directly by inspection of the actual two-point correlation functions themselves. A logarithmically binned version of the correlation functions for pure and perturbed Hubble flows is shown in Figure 7. The absorber-galaxy correlation function was generated using the total Lyα sample and the cone galaxy sample. The correlation functions were normalized in the usual way, using random samples with the selection function shown in Figure 3. The error bars were estimated using the formulae in Mo, Jing, & Borner (1992). As expected, the pure and perturbed Hubble flow models agree fairly well for separations larger than one or two megaparsecs; the perturbed Hubble flow model produces more very close pairs, since even small velocity differences wipe out small separations for the pure Hubble flow model. In both cases, the absorber-galaxy correlation is clearly weaker than the galaxy-galaxy correlation on scales from about 1 to 10 Mpc. However, although visual inspection of the absorber-galaxy correlation function may suggest that the correlation is significant out to about 10 Mpc, in fact the pair tests summarized in Table 5 and the nearest-neighbor tests summarized in Table 3 both indicate that a statistically significant absorber-galaxy correlation can be detected in our data sets only over volumes which are smaller than this.

3.4. *Some Particular Cases of Interest*

3.4.1. *The Closest Absorber-Galaxy Associations*

Actual associations between individual observed galaxies and absorbers in the 3C 273 sight line are difficult to prove for

TABLE 7

PAIR COUNT MONTE CARLO TESTS USING THE GALAXY DISTRIBUTION

Gal	Abs	Npair obs[a]	Npair monte[b]	Nmonte≤obs[c]
10 Mpc Pure Hubble Flow				
cylinder	total	1952	8562.7	0
cylinder	homogeneous	119	315.0	1
cylinder	strong	60	228.9	0
cone	total	98	245.8	0
cone	homogeneous	78	211.4	0
cone	strong	55	155.3	4
10 Mpc Perturbed Hubble Flow				
cylinder	total	1859	8121.9	0
cylinder	homogeneous	113	297.9	1
cylinder	strong	57	216.8	0
cone	total	98	231.7	0
cone	homogeneous	75	199.1	0
cone	strong	52	146.3	5

[a] Observed number of absorber-galaxy pairs within radius R (Mpc).

[b] Average of 1000 Monte Carlo numbers of absorber-galaxy pairs within radius R (Mpc).

[c] Number (out of 1000) of Monte Carlo tests with a *smaller* number of absorber-galaxy pairs within radius R. Thus the percentage probability of the observed value arising from a set of absorbers with the same distribution as the observed galaxies is this number divided by 10.

© American Astronomical Society • Provided by the NASA Astrophysics Data System

1993ApJ...419..524M

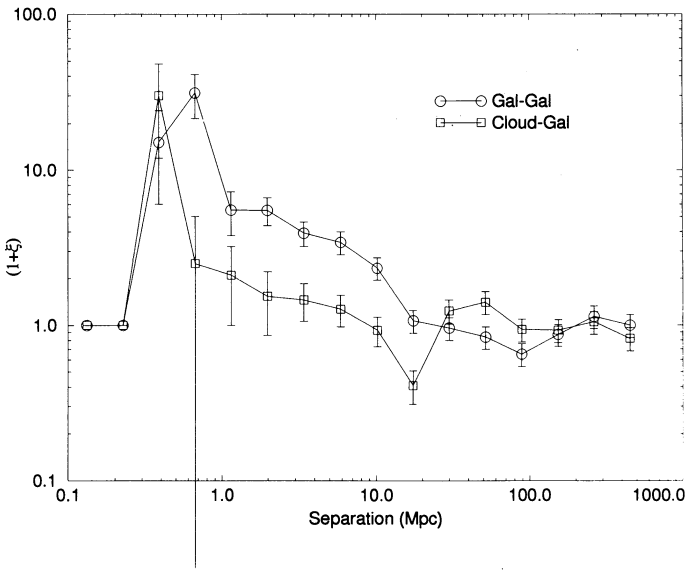

FIG. 7a

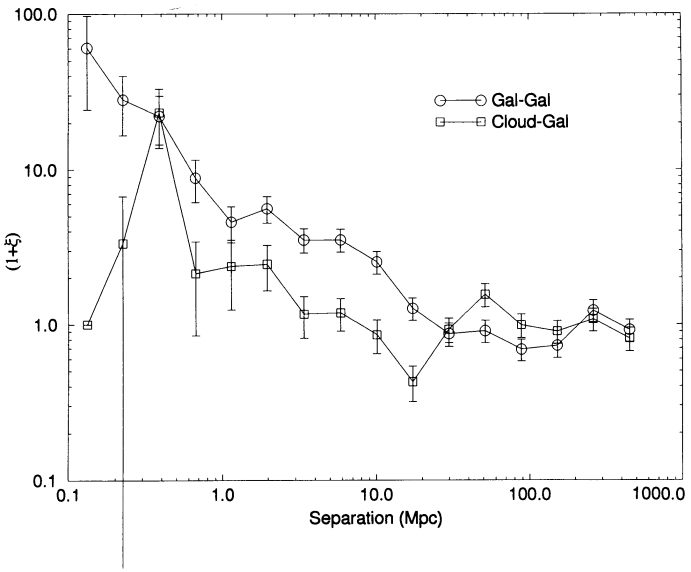

FIG. 7b

FIG. 7.—Two-point correlation functions of galaxy-galaxy and absorber-galaxy, (*a*) assuming pure Hubble flow and (*b*) assuming perturbed Hubble flow. See text, § 3.3.4.

a number of reasons: (1) The smallest projected distance to the 3C 273 line of sight of all the galaxies in our sample is still 160 kpc. (2) Galaxy rotation or velocity dispersions could produce velocity differences as large as 200 km s^{-1} between the mean galaxy velocity and an actually associated absorber (also comparable to the 3 σ error in our fiber data velocity measurements). (3) In regions of high galaxy density along the line of sight, peculiar motions of the galaxies and the absorbers in cluster potential wells may make the velocity-distance relationship complex. This is especially true of the Virgo region, and for the $z = 0.0034$ and $z = 0.0053$ absorbers (which also lie on the steep portion of the damping wings of the Galactic Lyα, and have only been observed at low resolution). With these caveats, it can be seen from Table 4 that the closest absorber-galaxy pair has a separation of 350 kpc (240 kpc). Outside the Virgo region (where the velocity-distance relationship may be less complex, but also where our galaxy sample goes to much less faint absolute magnitudes), the smallest separation is 410 kpc (350 kpc).

The best published example of an association between a Lyα absorber and a galaxy is given in Bahcall et al. (1992a), where a galaxy is found within 90 kpc of the sight line of H1821+643 which has a strong Lyα absorber (EW = 950 mÅ) within 400 km s^{-1}. There are no galaxies in our sample this close to the line of sight (or indeed any absorption systems this strong).

One can (somewhat arbitrarily) divide the absorbers in our sample into two groups: (1) Those with a galaxy within 1 Mpc of the line of sight, and with a velocity difference of less than 400 km s^{-1} (all of the Virgo systems and six of the higher redshift systems). Despite its entry in Table 4, the absorber at $z = 0.02622$ actually has two galaxies within 400 km s^{-1} and 1 Mpc projected separation. They do not appear in the table, since their large velocity differences (greater than 250 km s^{-1}) make their separation large, assuming pure Hubble flow. (2) The rest of the absorbers (eight systems). There is no significant difference in the EW distribution of these two samples.

Our data can also be used to consider the question, What is the average galaxy diameter within which one would see a neutral hydrogen column density of at least 10^{13} cm^{-2}? In practice this is rather a naive question, since the cross section almost certainly depends on galaxy luminosity and probably also morphology. One might also expect a patchy distribution of neutral hydrogen in the outer parts of galaxies leading to a covering factor not equal to unity. Nevertheless, ignoring these complications, and excluding the Virgo velocity range because of (*a*) the possibility of large peculiar velocities, (*b*) a wish to avoid the large range of intrinsic galaxy luminosities in the sample, and (*c*) the fact that because our absorber EW limit is higher in this region, we find that of the 12 galaxies with projected separation to the line of sight less than 1 Mpc, eight show Lyman absorption systems within 400 km s^{-1}. A velocity difference of up to about 400 km s^{-1} could possibly be attributed to internal motions within a large galaxy, coupled with our measuring error, or alternatively to a small group. Having eight or more such matches would occur 0.6% of the time if the absorbers were randomly distributed in velocity space. However, of these eight galaxies, two are associated with the absorber at $z = 0.02622$, and three with the absorber at $z = 0.2933$. Clearly several distinct galaxies cannot be producing the same absorber, and so in fact only five of the 12 systems within 1 Mpc of the line of sight to the quasar can be legitimately associated with individual absorbers. Reducing the projected separation to 500 kpc, one finds three galaxies, with velocity separations of 20, 120, and 0 km s^{-1} (see Table 3). This may be interpreted as saying that the cross section of galaxies with luminosities greater than $0.1L^*$ for log $N_{HI} > 10^{13}$ is between 0.5 and 1 Mpc, although by the phrase "cross section" we do not imply that the absorbers are necessarily associated with the actual galaxy in question.

Because of the three Virgo absorbers, all of the Virgo galaxies have an absorber within 400 km s^{-1}. However, it is clearly unreasonable to suggest that more than one galaxy is associated with a given absorber. Thus, of the 19 Virgo galaxies within 500 kpc of the line of sight, 16 must not be producing absorption. Of these 19, two have absolute magnitudes brighter than $1/10L^*$, and so are consistent with the above statement,

© American Astronomical Society • Provided by the NASA Astrophysics Data System

1993ApJ...419..524M

despite the higher absorber EW limit, as long as only one of the galaxies with luminosity less than $0.1L^*$ is producing observed absorption.

3.4.2. *The Most Isolated Lyman-α Absorbers*

One of the stronger lines in our absorber sample is also the most isolated. Any galaxy brighter than -18 would be in our sample at the redshift of the isolated $z = 0.06655$ absorber. However, the nearest such galaxy has a projected separation of 4.75 Mpc and a velocity difference of 710 km s^{-1}, which corresponds to a spatial separation of 10 Mpc for both pure and perturbed Hubble flow models. Indeed, studying the galaxy distribution in Figure 5, the three absorbers with $0.060 < z < 0.07$ seem to lie in a "void" in the galaxy distribution. While it is certainly possible that these absorbers are associated with galaxies below our absolute magnitude limit, *these isolated absorbers are a clear demonstration that one cannot associate ALL low-redshift Lyα absorbers with luminous (L^*) galaxies.*

3.4.3. *The Absence of Lyman-α Absorbers in the $z \sim 0.078$ Galaxy Concentration*

The most striking feature of the observed galaxy redshift distribution is a concentration of galaxies centered at a redshift of $z \sim 0.078$. This excess is almost certainly associated with a structure which includes the galaxy cluster Abell 1564. This cluster has a tabulated center at $\alpha = 12^h32^m25^s$, $\delta = 2°7'11''$ (1950), giving it an offset of 89′ southwest of the 2C 273 sight line. This angle corresponds to a separation of 7.3 Mpc at the cluster distance. Abell 1564 is the closest Abell cluster to the 3C 273 sight line, but is only of richness class 0. Redshifts for two member galaxies are given in Metcalfe et al. (1989), giving an average cluster redshift of 0.0793. Selecting all galaxies in our fiber sample with redshifts between 0.07 and 0.085 (54 galaxies), one derives a mean redshift of 0.0781 with rms of 0.0021 (630 km s^{-1}). For comparison, selecting galaxies between redshifts of 0.15 and 0.17 (the cluster around 3C 273; see Fig. 3), one gets 24 galaxies with mean redshift 0.1581 and rms 0.0024 (720 km s^{-1}).

Despite the location of Abell 1564 to the southwest, the galaxies in the redshift slice 0.07–0.085 show a weak concentration to the northeast of the fiber field, although there are galaxies in all parts of the fiber area surveyed. If they are really part of a structure including A1564, the structure must have a size of at least 8 Mpc. However, the nearest Lyα absorber is 0.0095 from the peak in redshift space (or 2850 km s^{-1}, which is 4.5 times the rms from the mean of the concentration) and is at a distance of 36 Mpc from the center of the concentration. It thus seems unlikely that there are any observed Lyα absorbers in our line of sight which are physically associated with this concentration.

We can test a slightly different form of the hypothesis considered in § 3.3.4 (although we grant that its application to the $z \sim 0.078$ galaxy concentration involves post facto statistics), namely, What is the probability that, if the Lyα absorbers are distributed in space "in the same way" as the galaxies in our sample, we should find the observed number of Lyα absorbers (none, in our case)? By "in the same way" we mean that

$$\frac{\rho_{\mathrm{Ly}\alpha}(r)}{\overline{\rho_{\mathrm{Ly}\alpha}}} = \frac{\rho_{\mathrm{galaxy}}(r)}{\overline{\rho_{\mathrm{galaxy}}}},$$

and by "in the vicinity of" we shall mean within $\pm 2.5 \times$ rms of the redshift peak of the concentration. We consider that our selection function can be meaningfully applied over the redshift range from about $z = 0.016$ out to our adopted "proximity cutoff" at $z = 0.151$. Carrying out the integration of our sample (i.e., the galaxy numbers weighted by the selection function) between $\pm 2.5 \times$ rms of the peak of the galaxy concentration and over the redshift range from 0.016 to 0.151, we find that *after correction for the selection function,* about 0.33 of an absolute-magnitude–limited cylindrical sample of galaxies should be found within 2.5 σ of the velocity peak of this structure. Since the Lyα absorbers are not subject to such a selection function, we can apply this equation to all the volume elements along the line of sight and, assuming further that the effective cross section of the Lyα absorbers (σ) is constant over the redshift range 0.016–0.151, one can write

$$n\sigma[(z_{\mathrm{peak}} + 2.5 \times \mathrm{rms}) - (z_{\mathrm{peak}} - 2.5 \times \mathrm{rms})] = 0.33\overline{n\sigma}(0.151 - 0.016).$$

This equation represents the number of Lyα absorbers in the vicinity of the peak that we should expect to see if our hypothesis is correct. Over the redshift interval 0.016–0.151 we have observed up to 14 Lyα absorbers, so that we expect $0.33 \times 14 \approx 4.7$ absorbers, and we observe none. The probability of this occurring is thus $\exp(-4.7) \approx 0.01$. This is not a strong result, because of the rather small number of absorbers expected and the post facto nature of the test as we acknowledged above, but is additional suggestive evidence that the Lyα absorbers do not follow the galaxy distribution and in particular that they may avoid strong concentrations of galaxies. It could be strengthened, of course, by observing additional lines of sight through dense concentrations.

It would be nice to repeat the above calculation for the case of the three absorbers found in the Virgo velocity region. However, there are a number of reasons why any estimate of the probability of finding three absorbers in this region with an apparent overdensity of galaxies is highly uncertain. First, our absorber sample is incomplete in this velocity range, as described in § 3.3.1. Second, the area of sky surveyed is so small that the selection function correction of this velocity range is very large. Taking our selection function at face value, the eight galaxies actually in our survey at Virgo velocities imply that 60% of an absolute-magnitude–limited cylindrical galaxy sample from $z = 0$ to $z = 0.151$ would be found in that velocity range. Our hypothesis above would then predict that (neglecting the incompleteness of the absorber sample) one would expect $0.6 \times 17 \approx 10$ absorbers, when we only see three. Unfortunately, it is not possible to place a meaningful uncertainty on this apparent underdensity of absorbers in the Virgo region, for the reasons listed above.

In summary, there is marginal evidence, both from a clump of galaxies at $z = 0.078$ and from the Virgo velocity range, that Lyα absorbers are less common in regions of high galaxy density.

4. SUMMARY AND DISCUSSION

We have assembled several types of observations in an attempt to find objects with which the Lyα absorbers along the line of sight of 3C 273 might be associated, and in order to carry out statistical tests of galaxy-Lyα absorber association. In particular, we obtained narrow-band images centered on and off the expected position of an Hα emission which might be associated with three of the low-redshift Lyα absorbers, and obtained deep broad-band images of a 17′ × 17′ field centered

© American Astronomical Society • Provided by the NASA Astrophysics Data System

1993ApJ...419..524M

on 3C 273. Both of these searches were negative. Our failure to identify any broad-band or Hα emission from plausible "galaxy-like" objects a few tens of kiloparsecs from the 3C 273 sight line at the approximate distance of the Virgo Cluster is being checked by more sensitive and extensive searches for Hα by T. Williams (1993, private communication) and 21 cm emission by van Gorkom (1993) and van Gorkom et al. (1993).

We have also obtained redshifts for a large number of galaxies in the vicinity of the 3C 273 sight line. Again, we find no unambiguous instance of association of any of the Lyα absorbers with individual galaxies. We define a number of samples for both the Lyα absorbers and the galaxies and estimate the three-dimensional separation between each galaxy-galaxy pair and each Lyα absorber-galaxy pair based upon two models for converting the observed redshift difference between any pair into a radial separation, viz., (1) the assumption of a pure Hubble flow and (2) a statistical model of "perturbed" Hubble flow based upon work of Davis & Peebles (1983). The resulting database is used to carry out statistical tests to confirm or reject two null hypotheses about the association of galaxies and Lyα absorbers, namely, (1) the Lyα absorbers show no tendency to cluster around galaxies, and (2) the Lyα absorbers cluster around galaxies exactly as the galaxies cluster about each other. While neither of these two hypotheses can be unambiguously rejected in the sense that every combination of samples and flow hypotheses reject both of them at significant levels, the evidence from these tests, and from the galaxy-galaxy and Lyα absorber-galaxy two-point correlations themselves, points quite strongly to the conclusion that both hypotheses are false.

In particular, over length scales from about 1 to 10 Mpc there seems little doubt that the Lyα absorbers cluster around galaxies less strongly than the galaxies themselves cluster. This is borne out by an examination of a redshift interval centered at about $z = 0.078$ at which a strong concentration of galaxies occurs but in the neighborhood of which there are no Lyα absorbers. Additionally, we find at least one Lyα absorber for which no galaxy with absolute magnitude brighter than about -18 can be found closer than about 5 Mpc. Taken together, all this evidence suggests that the most significant conclusion we have reached is that *the majority of low-redshift Lyα absorbers are not intimately associated with normal luminous galaxies.*

In view of the fact that it has long been realized that at high redshifts there is an absence of power in the Lyα absorber two-point correlation function in redshift space, except possibly at the very smallest velocity separations, this conclusion is not too surprising. On the other hand, it is also fairly clear that there is *some* tendency of the Lyα absorbers to cluster around galaxies, and even weak evidence that this clustering becomes strong at very small separations. Also, Bahcall et al. (1992a) have investigated the autocorrelation function of the low-redshift absorbers seen in the line of sight to H1821+643, and show that there is only a 4% probability that the observed "clumping" arose from a randomly distributed sample.

None of the foregoing points unambiguously, in our estimation, to a particular model for the formation and evolution of the Lyα absorbers. As have others, we simply offer the following speculations which appear to be compatible with the facts as they are presently understood.

At high redshifts, the Lyα absorbers consist primarily of entities which are only very loosely associated with larger mass objects (e.g., proto-galaxies) and which are evolving fairly rapidly. Possibly this dominant population consists of absorbers in which gravitational binding (e.g., by dark matter) plays no significant role. In addition to this group, there is a smaller population of absorbers which are evolving less rapidly, possibly stabilized by dark matter, and which are clustered more strongly about galaxies. At very low redshifts, this latter population is beginning to constitute a large enough fraction of the absorbers that power in the two-point correlation function is detectable. Thus, the present mix of Lyα absorbers appears to have clustering properties intermediate between present-epoch normal galaxies and a random non-clustered population. This property also appears to be shared by the low-luminosity, moderate-redshift "blue galaxies" (Pritchet & Infante 1992), leading to the plausible conjecture that the Lyα absorbers are more closely related to low-mass, low-luminosity galaxies than they are to L^* galaxies, although the relation is clearly not one-to-one.

We have no good way at present of estimating the characteristic scale or masses of the low-redshift Lyα absorbers. A guess at a diameter of 30 kpc is as plausible as any. In particular, consider a pancake whose diameter is 30 kpc and whose thickness is 10 kpc. In this case, at the present epoch, a hydrogen column density of 10^{13}–10^{14} cm^{-2} normal to the face of the absorber, coupled with estimates for the present-epoch energy density of ionizing radiation leads to a total gas mass of order $10^7\ M_\odot$, but a mass of only a few hundred solar masses of *neutral* hydrogen. It is of interest that the mass function of neutral hydrogen gas clouds appears to be truncated below about $10^8\ M_\odot$ (Weinberg et al. 1991). As Maloney (1992, 1993) has shown, the gas in a flaring galaxy with decreasing column density will undergo a rather sudden transition along this face from being mostly neutral to mostly ionized, with the consequence that few if any contours with neutral hydrogen column density of order 10^{18} cm^{-2} are known. Similarly, it is conceivable that, given the appropriate run of length scale with mass, a sequence of masses would have the property of making a sudden transition in the mass function of neutral hydrogen starting at about $10^8\ M_\odot$, leading to a dearth of objects with total H I masses for several orders of magnitude below this.

If these speculations have any connection with reality, then one might expect to see some similarity in the clustering properties of the Lyα absorbers and low-mass galaxies. We are currently attempting to obtain redshifts of galaxies of lower luminosity along the 3C 273 sight line in order to investigate this possibility.

We would like to thank Greg Aldring and Steve Shectman for help and advice in using the LCO fiber system, Neil Reid for giving us access to one of the new Palomar Sky-survey plates, Allan Sandage for allowing us to inspect one of his older IIIa-J plates, Mark Davis and Margaret Geller for advice on generating Monte Carlo samples with known correlation functions, Don Schneider for help with the JASON software, and Xavier Barcons, Donald Lynden-Bell, Mario Mateo, Houjon Mo, Michael Rauch, John Webb, Jeff Willick, and Dennis Zaritzky for useful conversations. We would also like to thank the referee, J. N. Bahcall, for his helpful and constructive comments which improved the content and presentation of the paper. S. L. M. and R. J. W. acknowledge support through NASA contract NAS5-30101 and NSF grant AST-9005117.

© American Astronomical Society • Provided by the NASA Astrophysics Data System

1993ApJ...419..524M

REFERENCES

Allen, C. W. 1973, Astrophysical Quantities (3d ed.; London: Athlone)
Bahcall, J. N., et al. 1993, ApJS, 87, 1
Bahcall, J. N., Jannuzi, B. T., Schneider, D. P., Hartig, G. F., Bohlin, R., & Junkkarinen, V. 1991a, in The First Year of *HST* Observations, ed. A. L. Kinney & J. C. Blades (Baltimore: STScI), 46
———. 1991b, ApJ, 377, L5
Bahcall, J. N., Jannuzi, B. T., Schneider, D. P., Hartig, G. F., & Green, R. F. 1992a, ApJ, 397, 68
Bahcall, J. N., Jannuzi, B. T., Schneider, D. P., Hartig, G. F., & Jenkins, E. B. 1992b, ApJ, 398, 495
Binggeli, B., Sandage, A., & Tammann, G. A. 1985, AJ, 90, 1681
Brandt, J. C., et al. 1993, AJ, 105, 831
Chernomordic, V. V., & Ozernoy, L. L. 1983, Nature, 303, 153
Davis, M., & Peebles, P. J. E. 1983, ApJ, 267, 465
Fransson, C., & Epstein, R. 1982, MNRAS, 198, 1127
Huchra, J. P. 1990, CfA Redshift Catalog, 1990 May 5 version, obtained through the Astronomical Data Center
Jacoby, G. H., et al. 1992, PASP, 104, 599
Kennicutt, R. C. 1984, ApJ, 287, 116
Kent, S. M. 1985, PASP, 97, 165
Loveday, J., Peterson, B. A., Efstathiou, G., & Maddox, S. J. 1992, ApJ, 390, 338
Maloney, P. 1992, ApJ, 389, L89
———. 1993, ApJ, 414, 41
Massey, P. 1990, NOAO Newsletter, No. 21 (1990 March)
Mo, H. J., Jing, Y. P., & Borner, G. 1992, ApJ, 392, 452
Mo, H. J., Einasto, M., Xia, X. Y., & Deng, Z. G. 1992, MNRAS, 255, 382
Mo, H. J., & Morris, S. L. 1993, in preparation
Metcalfe, N., Fong, R., Shanks, T., & Kilkenny, D. 1989, MNRAS, 236, 207
Morris, S. L., Weymann, R. J., Savage, B. D., & Gilliland, R. L. 1991, ApJ, 377, L21
Osterbrock, D. E. 1989, Astrophysics of Gaseous Nebulae and Active Galactic Nuclei (Mill Valley: University Science Books)
Phillips, S., Disney, M. J., & Davies, J. I. 1993, MNRAS, 260, 453
Pritchet, C. J., & Infante, L. 1992, ApJ, 399, L35
Rauch, M., Carswell, R. F., Caffee, F. H., Foltz, C. B., Webb, J. K., Weymann, R. J., Bechtold, J., & Green, R. F. 1992, ApJ, 390, 387
Salzer, J. J. 1992, AJ, 103, 385
Sandage, A., & Binggeli, B. 1984, AJ, 89, 919
Savage, B. D., Lu, L., Weymann, R. J., Morris, S. L., & Gilliland, R. L. 1993, ApJ, 404, 124
Schneider, D. P., et al. 1993, ApJS, 87, 45
Shectman, S. A. 1992, in ASP Conf. Ser. 37, Fiber Optics in Astronomy II, ed. P. M. Gray (San Francisco: ASP), 26
Songaila, A., Bryant, W., & Cowie, L. L. 1989, ApJ, 345, L71
Stockton, A. 1980, in IAU Symp. 92, Objects of High Redshift, ed. G. O. Abell & P. J. E. Peebles (Dordrecht: Reidel), 87
van Gorkom, J. H. 1993, in Proc. Grand Teton National Park Wyoming Conf., ed. M. Shull & H. Thronson (Dordrecht: Kluwer), in press
van Gorkom, J. H., Bahcall, J. N., Jannuzi, B., & Schneider, D. 1993, AJ, in press
Vilas, F., & Smith, B. A. 1987, Appl. Optics, 26, 4
Weinberg, D. H., Szomoru, A., Guhathakurta, P., & van Gorkom, J. H. 1991, ApJ, 372, L13

© American Astronomical Society • Provided by the NASA Astrophysics Data System